AN ABSTRACT OF THE THESIS OF

Hailey M. Murdock for the degree of Master of Science in Materials Science
presented on October 29, 2010

Title: Processing Effects on the Ductility of Chromium-Vanadium Alloys

Abstract approved:

Jamie Kruzic

The next generation of high temperature structural alloys must exhibit exceptional resistance to fracture, creep, oxidation, and fatigue at high temperatures. Chromium is being considered due to its high melting point (>1800°C), relatively low density (~7.2 g/cc), high temperature strength, and oxidation resistance. Limiting the use of chromium is its high ductile-to-brittle transition temperature. Previous efforts to reduce the ductile-to-brittle transition temperature have considered elimination of embrittling interstitals, increasing the grain size, pre-deformation and alloying. Recent computational studies have renewed interest in using alloying additions to ductilize chromium. A series of first principles calculations recently revealed elements (Ti, Zr, Hf, Nb, V) which have potential to reduce the ductile-to-brittle transition temperature when alloyed with chromium. To experimentally measure the effects of alloying and processing on the ductile-to-brittle transition temperature, chromium-vanadium alloy samples of 3 different compositions were prepared and compared to nominally pure chromium.

Chromium vanadium samples were prepared from powders, hot isostatically pressed, heat treated at 1300°C and extruded at 1200°C. Elevated temperature Vickers hardness, elevated temperature tensile and elevated 3-point bend tests were performed. A diffusion study was performed using microprobe analysis to assist in the development of homogenization procedures for the alloys. Fracture surface

analysis of bend and tensile specimens was used to determine the mode of fracture in bend and tensile specimens. Elevated temperature tensile tests determined a relationship between temperature and ductility in 100%Cr and 25%Cr-75%V alloys.

Results from elevated temperature Vickers hardness suggest alloying with vanadium increases the strength by a factor of two. Premature failure in elevated temperature 3-point bend specimens and elevated temperature tensile tests made it difficult to quantify the effect of vanadium in affecting the ductility of chromium. Electron microscopy observations indicate that mechanical damage, likely caused by extrusion, is responsible for initiating the premature failures. Despite this complication, evidence of micro- and macro-scale ductile fracture mechanisms on the fracture surfaces of the Cr-V alloys indicate that the addition of vanadium indeed improves the ductility of chromium.

Processing Effects on the Ductility of Chromium-Vanadium Alloys

by
Hailey M. Murdock

A THESIS

submitted to

Oregon State University

in partial fulfillment of
the requirements for the
degree of

Master of Science

Presented October 29, 2010
Commencement June 2011

Master of Science thesis of Hailey M. Murdock

presented on October 29,2010.

APPROVED:

Major Professor, representing Materials Science

Head/Chair of the Department of Materials Science

Dean of the Graduate School

I understand that my thesis will become part of the permanent collection of Oregon State University libraries. My signature below authorizes release of my thesis to any reader upon request.

Hailey M. Murdock, Author

ACKNOWLEDGEMENTS

It is a pleasure to thank those individuals whose help and support made this thesis possible:

Dr. Jay Kruzic and Dr. Omer Dogan for their encouragement and guidance during this process enabled me to develop an intimate understanding of this subject.

Neil Duttlinger for the generous use of his test equipment, time and stereo

Dr. Frank Tepley III for providing his assistance and expertise during the use of the electron microprobe

Dr. Yi Liu for assistance with microscopy and sample preparation

Joe Ferron for data analysis

Dr. Bill Warnes for his guidance and support

Dave Percival for patience, support and understanding while I progress through my educational endeavors

Finally, I would like to thank my family and friends for their undying wisdom and support during the last few years, it has truly helped me get to where I am today

and

The Department of Energy for funding this project

TABLE OF CONTENTS

Page

1.0 Introduction 1

2.0 Background 3

2.1 Niobium Silicide Alloys 7

2.2 Molybdenum Silicide Alloys 8

2.3 Chromium 9

2.3.1 Oxidation and Corrosion Resistance 10
2.3.2 Ductile-To-Brittle Transition Temperature 11
2.3.3 Grain Size Effects 12
2.3.4 Impurity Effects 13
2.3.5 Pre-Deformation Effects 15
2.3.6 Alloying Additions 16

3. 0 Methods 19

3.1 Sample Preparation 19

3.2 Microstructure 21

3.2.1 Optical Microscopy and Grain Size Analysis 21
3.2.2 X-Ray Diffraction 21
3.2.3 Microprobe Analysis 21

3.3 Mechanical Testing 23

3.3.1 Elevated Temperature Vickers Hardness 23
3.3.2 Elevated Temperature 3-Point Bend 23
3.3.3 Elevated Temperature Tensile Test 27
3.3.4 Fracture Surface Analysis 27
3.3.5 Stress Intensity Factor Calculations 28

4.0 Results 31

4.1 Microstructure 31

4.1.1 Optical Microscopy and Grain Size Analysis 31
4.1.2 X-Ray Diffraction 34
4.1.3 Microprobe Analysis 37

4.2 Mechanical Testing 41

TABLE OF CONTENTS (Continued)

Page

4.2.1 Elevated Temperature Vickers Hardness....41
4.2.2 Elevated Temperature 3-Point Bend Testing....44
4.2.3 Elevated Temperature Tensile Testing....49

4.3 Fracture Surface Analysis....53

4.3.1 100 Cr 3-Point Bend Fracture Surfaces....53
4.3.2 75Cr-25V 3-Point Bend Fracture Surfaces....55
4.3.3 50Cr-50V 3-Point Bend Fracture Surfaces....57
4.3.4 25Cr-75V 3-Point Bend Fracture Surfaces....59
4.3.5 100Cr Elevated Temperature Tensile Fracture Surfaces....61
4.3.6 25Cr-75V Elevated Temperature Tensile Fracture Surfaces....62
4.3.7 75Cr-25V Elevated Temperature Tensile Fracture Surfaces....63

4.4 Fracture Toughness Calculations....63

5.0 Discussion....65

5.1 Processing....65

5.2 Mechanical Testing....65

5.2.1 Pure Chromium Samples....66
5.2.2 Chromium Vanadium Samples....66
5.2.3 75Cr-25V Samples....67
5.2.4 50Cr-50V and 25Cr-75V Samples....67

6.0 Conclusions....69

References....71

LIST OF FIGURES

Figure — Page

Figure 2.1: Power versus Rotor Temperature for Turbine engines over the Past 70 Years…… 4

Figure 2.2: Density Normalized Tensile Strength Versus Temperature……... 5

Figure 2.3: Metal Recession (μm/h) of Niobium In-Situ Composites at 1200°C 7

Figure 2.4: Creep Rates of Selected Niobium Silicides Plotted Against Applied Stress……. 8

Figure 2.5: Mass Loss of Molybdenum at High Temperatures…… 9

Figure 2.6: Representative Charpy Impact Ductile-To-Brittle Transition Curve 11

Figure 2.7: Effect of Grain Size on The Room-Temperature Yield Stress……... 12

Figure 3.1: 3-point Bend Test Specimen Dimensions…….. 24

Figure 3.2: *3-point* Bend Beam Diagrams…… 26

Figure 3.3: Tensile Specimen……... 27

Figure 3.4: Surface Crack in a Finite Plate……... 28

Figure 4.1: Optical Microscopy Showing Microstructure of Heat Treated Samples a) 100Cr b) 50Cr-50V c) 75Cr-25V d) 25Cr- 75V……. 31

Figure 4.2: Optical Microscopy Showing the Transverse Direction of Extruded Samples Images Taken at 100X a) 100Cr b) 50Cr-50V c) 75Cr-25V d) 25Cr- 75V……. 32

Figure 4.3:Optical Microscopy Showing the Longitudinal Direction of Extruded Samples a)100Cr (200X) b)75Cr-25V (100X) c)50Cr-50V (100X) d)25Cr-75V(100X) ……..... 33

Figure 4.4: X-Ray Diffraction Results as a Function of Processing History a) 100-Cr b) 50Cr-50V c) 75Cr-50V d) 25Cr-75V……... 36

Figure 4.5: 50Cr-50V As-Hot Isostatically Pressed Concentration Vs. Position Profile taken at 1.0 μ Step-Size…… 37

Figure 4.6: 50Cr-50V After 120 Hours 1300°C Heat Treatment Sample 38

Concentration vs. Position Profile taken at 2.0 μ Step-Size…….
Figure 4.7: 50Cr-50V Extruded Sample Concentration vs. Position Profile Taken at 2.0 μ Step-Size……... 38
Figure 4.8: Calculated Concentration Profile Compared to Actual Concentration Profile…… 40
Figure 4.9: Vickers Hardness Versus Temperature With Linear Regression Fit a)100-Cr b)75Cr-25V c)50Cr-50V d)25Cr-75V……... 43
Figure 4.10: Load vs. Displacement Electropolished 100Cr…… 44
Figure 4.11: Load vs. Displacement Mechanically Polished 100Cr……. 45
Figure 4.12: Load vs. Displacement 75Cr-25V…… 46
Figure 4.13: Load vs. Displacement 50Cr-50V…… 47
Figure 4.14: Load vs. Displacement 25Cr-75V…… 48
Figure 4.15: Elevated Temperature Tensile Results 100-Cr……. 49
Figure 4.16: Elevated Temperature Tensile Results 75Cr-25V…… 50
Figure 4.17: Elevated Temperature Tensile Results 25Cr-75V…… 51
Figure 4.18: Reduction in Area as a Function of Temperature for Elevated Temperature Tensile Specimens……... 52
Figure 4.19: Fracture surface of 100-Cr showing origin of fracture in elevated temperature *3-point* bend specimens a)180°C b)80°C c)80°C d)21°C (Mechanical Polish)…….. 53
Figure 4.20: Tensile surface of 100Cr elevated temperature *3-point* bend specimens a) 280°C b) 230°C c)380°C d)80°C (Mechanical Polish).. 54
Figure 4.21: Fracture surface of 75Cr-25V elevated temperature *3-point* bend specimens a)380°C-2 b) 330°C-2 c) 330°C-1 d) 380°C-1……... 55
Figure 4.22: Tensile Surface of 75Cr-25V Showing Yittra Stringers on Tensile Surface of 3-point Bend Specimens a) 380°C-2 b) 380°C-1 c) 330°C-1 d)330°C-1……. 56
Figure 4.23: Fracture surface of 50Cr-50V elevated temperature *3-point* bend specimens a) 280°C b) 380°C c) 330°C d) 180°C…… 57

Figure 4.24: Tensile surface of 50Cr-50V *3-point* bend specimens a)280°C b)380°C c)180°C d)380°C…… 58
Figure 4.25: Fracture Surface of 25Cr-75V *3-point* Bend Specimens a)280°C b)380°C c)180°C…….. 59
Figure 4.26: Tensile Surface of 25Cr-75VShowing Tensile Surfaces of *3-point* Bend Specimens a)180°C b)330°C c)230°C d)230°C…….. 60
Figure 4.27: Fracture Surface of 100-Cr Elevated Temperature Tensile Specimens a)230°C b)280°C c)180°C d)280°C……... 61
Figure 4.28: Fracture Surface of 25Cr-75V Elevated Temperature Tensile Specimens a)280°C b)180°C c)280°C d)80°C…….. 62
Figure 4.29: Fracture Surface of 75Cr-25V Elevated Temperature Tensile Specimen at 380°C …….. 63
Figure 4.30 Largest Surface Crack Found in the Unstressed Region of a 50Cr-50V Elevated Temperature *3-point* Specimen…….. 64

LIST OF TABLES

Table Page

Table 2.1: Properties of Refractory Materials…… 6

Table 3.1: Atomic% Composition of Powder Metallurgy Samples……... 19

Table 3.2: Leco Analysis Results……... 19

Table 3.3: Final Alloy Composition Determined by X-ray Fluorescence (wt%).. 20

Table 3.4: Time of Heat Treatments at 1300°C……. 20

Table 3.5: Dimensions of *3-point* Bend Specimens……... 27

Table 4.1: Mean Grain Diameter of Cr-V Samples After 120 Hour Heat Treatment…… 34

Table 4.2: Mean Grain Diameter of Cr-V Samples After Extrusion…….. 34

Table 4.3: Calculated Diffusivities for Cr into V at 1300°C…….. 39

Table 4.4: Summary Statistics of the Accuracy and Precision of Electron Microprobe……. 40

Table 4.5: Elevated Temperature (25°C -900°C) Vickers Hardness (GPa) Values for 120 Hour 1300°C Heat Treated (T5) Samples, (Standard Deviation)…….. 41

Table 4.6: Elevated Temperature (25°C -900°C) Vickers Hardness (GPa) for Extruded (T6) Samples, (Standard Deviation)……... 42

Table 4.7: Summary of Results for 100-Cr Elevated Temperature *3-point* Bend Tests…… 45

Table 4.8: Summary of Results for 75Cr-25V Elevated Temperature *3-point* Bend Tests…….. 46

Table 4.9: Summary of Results for 50Cr-50V Elevated Temperature *3-point* Bend Tests…….. 47

Table 4.10: Summary of Results for 25Cr-75V Elevated Temperature *3-point* Bend Tests…….. 48

Table 4.11: Summary of Results for 100-Cr Elevated Temperature Tensile Test. 49

Table 4.12: Summary of Results for 75Cr-25V Elevated Temperature Tensile 50

Test…….
Table 4.13: Summary of Results for 25Cr-75V Elevated Temperature Tensile Test……. 51
Table 4.14: Summary of Values Used for Fracture Toughness Calculations…… 64

Processing Effects on the Ductility of Chromium-Vanadium Alloys

1.0 Introduction

The use of refractory metal based materials in the hottest part of aerospace turbine engines has received considerable attention over the past decade. With current ferrous and non ferrous superalloys limited by low melting temperatures, considerable effort has been made to find the next generation structural alloy. Refractory metals have many desirable properties which make them promising candidates for new higher temperature alloys which can operate in aggressive environments. Some of the properties which are considered to be the most important for high temperature structural applications include:

- high strength at high temperatures
- superior creep resistance
- excellent oxidation resistance
- corrosion resistance
- resistance to thermal fatigue
- wear resistance
- low density
- ease of manufacturing
- low cost

Refractory alloys can provide the high melting temperatures and high strength values at high temperatures. Yet, issues with oxidation and creep resistance in molybdenum and niobium based alloys as well as cracking and brittle fracture at room temperature in chromium alloys, correlated to a high ductile-to-brittle transition temperature (DBTT), have ultimately limited their use.

Chromium is being considered here due to its high melting temperature (>1800°C), relatively low density (~7.2 g/cc), and high temperature strength at temperatures in excess of 1300°C. Moreover, chromium exhibits better oxidation/corrosion resistance, compared with other refractory materials, and is the most abundant refractory metal in the world making it more economical. Nonetheless, it is chromium's high DBTT which has significantly hindered its manufacturability. Issues of low oxidation and corrosion resistance at temperatures higher than 900°C have also hindered its large scale use.

A recent series of first principles calculations revealed five elements, including vanadium, to have a potentially ductilizing effect when alloyed with chromium, reigniting interest in chromium as a high temperature structural material. However, due to the high melting temperature of refractory metals, i.e., chromium and vanadium, manufacturability remains a challenge, and advanced processing techniques must be employed.

The ultimate goal of this research is to measure the effects of vanadium additions and processing history on the ductile-to-brittle transition curve of chromium. The effects of heat treating and extruding on the homogeneity and ultimately the elevated temperature *3-point* bend and tensile behavior of Cr-V alloys is evaluated.

2.0 Background

Over fifty years ago the development of aerospace turbine materials led to single crystal nickel based super alloys. Nickel and iron based superalloys are currently considered the industry standard for high temperature structural materials.[1] However, with a need for higher engine efficiencies and ultimately higher operating temperatures, current ferrous and non ferrous alloys are no longer sufficient as the operating temperatures have reached the maximum allowable temperatures for these alloys.[2, 3] Current performance of turbine engines can be best summarized by the power produced as a function of the turbine rotor inlet temperature. Figure 2.1 shows historical data for turbine aerospace engines for the past seventy years. While there is a general upward trend in engine performance, most of it can be attributed to advancements in cooling systems and coatings.[2] The losses due to inefficiency is attributed to the cooling air which must be passed through the compression section of the engine to prevent the nickel based alloys from melting.[3] Therefore, simply increasing the operating temperature (or decreasing the need for cooling air) will have a significant impact on the efficiency of these engines.[3]

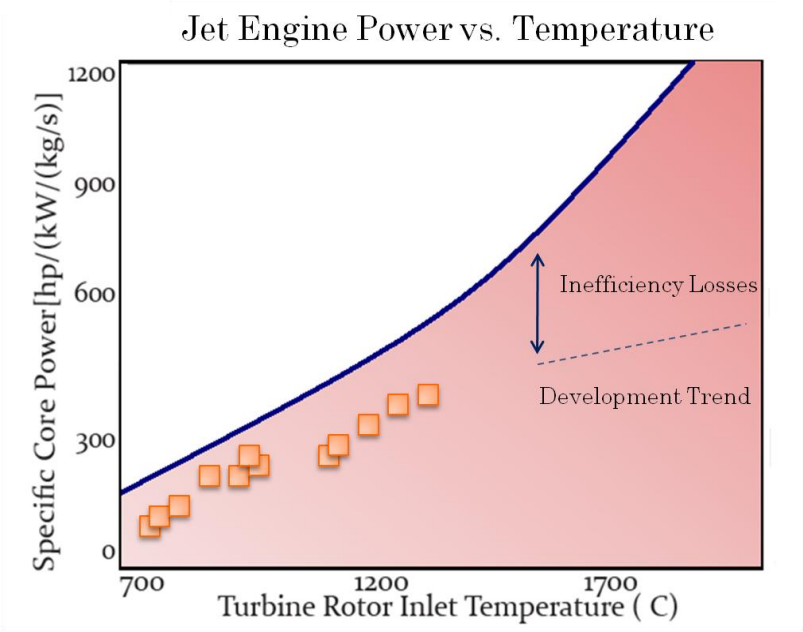

Figure 2.1: Power versus Rotor Temperature for Turbine engines over the Past 70 Years. Data Taken From Reference [2]

With the need for higher temperatures there has been a renewed interest in refractory metals as they provide the high strength at high temperatures required. Refractory metals have been considered for high-temperature structural applications since the 1950's, when initial research on superalloys was being performed. For refractory alloys to be used in future turbine engines, they will have to outperform the current nickel and iron based superalloys.[2] Figure 2.2 shows strength versus temperature for refractory metals compared with a nickel-based superalloy.

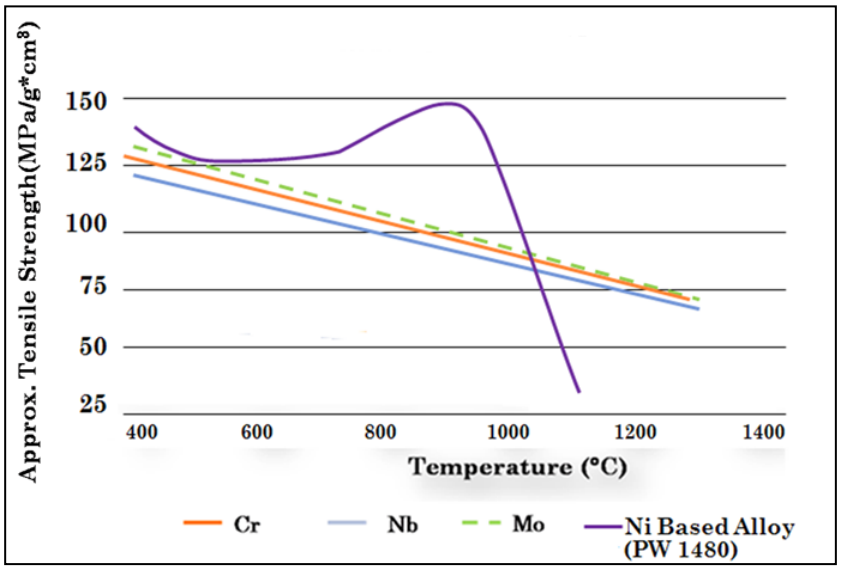

Figure 2.2: Density Normalized Tensile Strength Versus Temperature. Data Taken From Reference [4]

As can be seen from the figure nickel based superalloys quickly lose strength around 1000°C, while refractory metals Cr, Nb, and Mo provide higher strength at higher temperatures.

Critical to the development of refractory alloys is their strength, corrosion, oxidation and fatigue resistance at high temperatures and ductility at room temperature. Refractory metals niobium, chromium, molybdenum, tungsten, rhenium, tantalum, and vanadium are generally characterized by their high strength, and high melting point; making them ideal candidates for the next generation of high temperature structural alloys.[4, 5] Table 2.1 provides a quick overview of the properties of refractory metals compared to nickel.

Table 2.1: Properties of Refractory Materials. Data Taken From Reference [4]

Element	Modulus of Elasticity (GPa)	Melting Point (C°)	Density (g/cc)	Structure
Ni	170	1453	8.9	FCC
V	128	1902	5.8	BCC
Nb	105	2468	8.6	BCC
Ta	186	2966	16.7	BCC
Cr	279	1857	7.19	BCC
Mo	329	2617	10.3	BCC
W	411	3410	19.3	BCC
Re	463	3180	21.0	HCP

Constraining the use of refractory elements has been low oxidation resistance, poor creep resistance and high ductile-to-brittle transition temperatures.[4] Additionally, the elements with the highest melting temperatures and highest strength also have the highest densities as shown in Table 2.1. Of the refractory alloys Nb and Mo are currently considered to have the highest potential for turbine applications.[3]

2.1 Niobium Silicide Alloys

Relying on niobium's inherent room temperature ductility and relatively low density (8.56 g/cc), niobium-based composites represent a promising refractory-based system. These composites have excellent high and low temperature mechanical properties, mostly attributed to a niobium based metallic toughening phase.[6] Furthermore, alloying additions titanium, chromium, hafnium and aluminum have substantially improved niobium's low oxidation resistance above 500°C.[3, 4] Unfortunately, many of the elements which increase oxidation resistance also increase the creep rate. Therefore, balancing the high temperature oxidation resistance with creep resistance is the current focus of research on these alloys.[4]

Niobium intermetallic in-situ composites (e.g., Nb-19Ti-4Hf-13Cr-2Al-4B-16Si), are the prevailing class of niobium based alloys which exhibit both superior oxidation resistance and improved creep resistance. Figure 2.3 shows Niobium intermetallic in-situ composites, exhibiting a significant increase in the oxidation resistance with alloy development. Figure 2.4 shows the creep rate for these materials. As can be seen from the two figures oxidation resistance has been achieved but the addition of hafnium and titanium has increased the creep rate beyond what is acceptable.

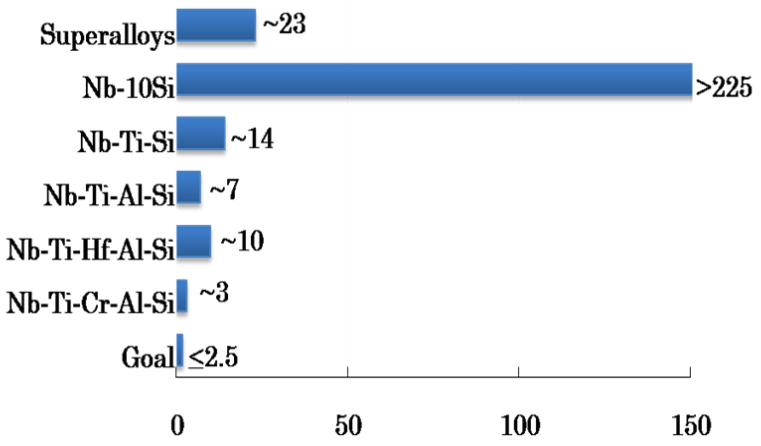

Figure 2.3: Metal Recession (μm/h) of Niobium In-Situ Composites at 1200°C. Data Taken From Reference [4]

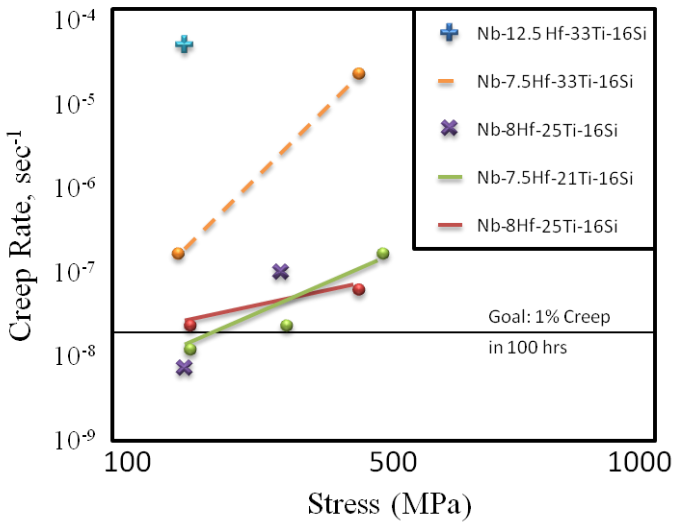

Figure 2.4: Creep Rates of Selected Niobium Silicides Plotted Against Applied Stress. Data Taken From Reference [4]

For niobium alloys to successfully integrate into the aerospace industry, the composition must be optimized to obtain the right combination of strength, oxidation resistance and creep resistance.[4]

2.2 Molybdenum Silicide Alloys

In addition to niobium alloys, molybdenum alloys hold considerable promise for high temperature structural applications if issues related to volatile oxide formation can be remedied.[7] Molybdenum based alloys such as TZM (Mo-.05Ti-.08Zr-.03C) are established high-temperature refractory materials primarily for operation in inert environments.[1] However, these alloys suffer from a volatile oxide formation of MoO_3 at temperatures between 700°C-1100°C (Figure 2.5). Additions of aluminum or silicon to produce the thermodynamically stable Al_2O_3 (alumina) or SiO_2 (silica) films have been shown to dramatically increase the oxidation resistance of the underlying material.[8]

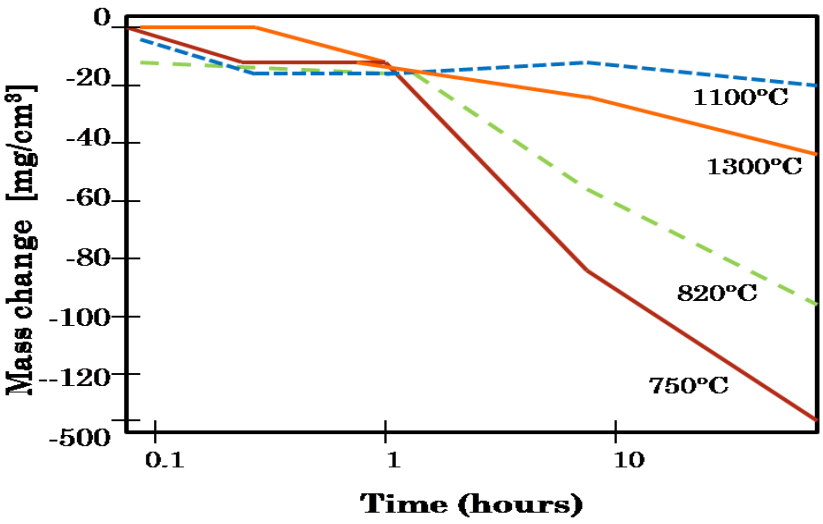

Figure 2.5: Mass Loss of Molybdenum at High Temperatures. Data Taken From Reference [9]

In 1997, Berczik received a patent for a group of Mo-Si-B alloys in the range of 1.6-15.2at% Si and 0.0-39.4 at% B. His approach was to produce a composite material with dispersed molybdenum borosilicide particles. The Mo silicide material utilizes the oxidation resistance of Mo_3Si and Mo_5SiB_2 phases leading to a surface formation of borosilicate glass layers.[8] Favorable mechanical properties of these alloys are assumed to be mainly imparted by the molybdenum matrix. These alloys rely on silicon boride intermetallics for high temperature oxidation resistance yet they strongly embrittle the molybdenum matrix, and much of the current research on these alloys has been directed at balancing mechanical properties with oxidation resistance.

2.3 Chromium

Due to its relatively high resistance to creep, relatively low density (~20% less than nickel), high strength at high temperatures, low cost and ease of hot working chromium has been identified as a promising refractory material for next

generation high temperature structural alloys. Limiting the use of chromium has been its high ductile-to-brittle transition temperature, low fracture toughness at room temperature, and poor oxidation/corrosion resistance at elevated temperatures (compared with nickel based superalloys).[10]

2.3.1 Oxidation and Corrosion Resistance

Oxidation and corrosion resistance is a chief requirement for structural alloys for high temperature applications. The operating temperatures of aerospace turbine engines in air are in excess of 1100°C. Traditionally, engine materials are protected with sophisticated thin coatings, to provide superior resistance to corrosion and oxidation during high temperature service.[11] Many refractory alloys including chromium oxidize very rapidly, well below their melting temperature. The primary mechanism of oxidation and corrosion resistance is to form a thin oxide layer on the surface to protect the bulk material. By forming a dense surface scale of Cr_2O_3, chromium demonstrates exceptional resistance to corrosion compared to other refractory metals. Below 900°C, this scale is stable and does not readily oxidize to its highest oxidation state (CrO_3) which is volatile above 900°C.[12, 13]

Alloying additions to chromium can provide additional oxidation and corrosion resistance that is equivalent to, or even exceeding, that required by current aircraft engine technologies.[4] Efforts by Oryshich et. al, have shown that small additions of rare earths such as La and B have a large impact on the 900°C oxidation resistance of hot isostatically pressed powder metallurgy samples.[12] Other research performed by Portini et. al. suggests that dispersing MgO particles increases oxidation and corrosion resistance of chromium at high temperatures.[14] While considerable progress has been made towards improving the corrosion and oxidation resistance; it is the room temperature mechanical properties that are the largest barrier to entry for chromium.

2.3.2 Ductile-To-Brittle Transition Temperature

High ductile-to-brittle transition temperature of commercially pure chromium has made manufacturability of chromium alloys difficult. The ductile-to-brittle transition temperature (DBTT) is defined as the temperature range over which a material transitions from brittle fracture to ductile fracture; and therefore the transition can be characterized by a thorough examination of the fracture surface of test specimens. Figure 2.6, shows a representative ductile-to-brittle transition curve obtained by Charpy Impact testing. For chromium this transition occurs around 300°C. To be considered for turbine applications, the DBTT would have to be lowered below room temperature.

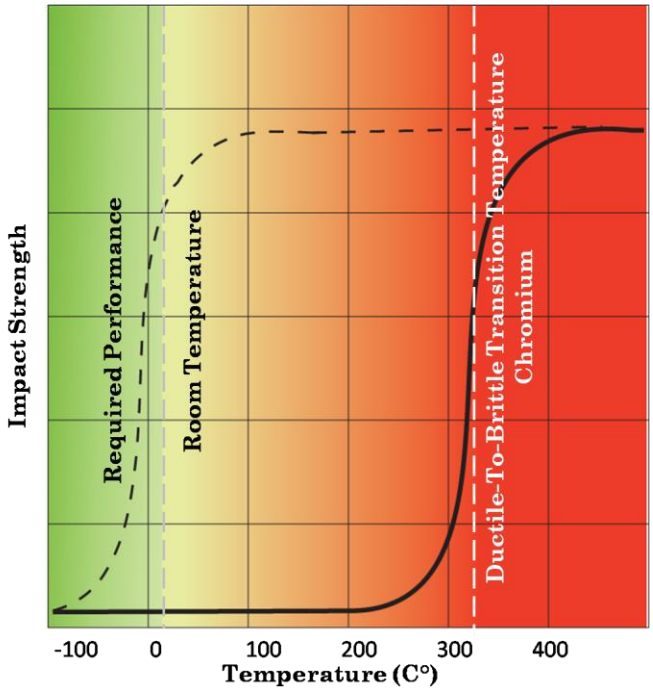

Figure 2.6: Representative Charpy Impact Ductile-To-Brittle Transition Curve

Several theories have been proposed as a means to control the low temperature brittleness of commercially pure chromium.[15] 1) It has been shown that brittleness in chromium may be controlled by the amount of grain boundary impurities and orientation of grains; as wrought chromium with high nitrogen impurities and a fibered grain structure is ductile compared to recrystallized

chromium with similar nitrogen contamination.[15] 2) Pre-straining (2%-8%) can significantly reduce the DBTT.[16] 3) Finally, many alloying additions have been proposed yet there is currently no alloying addition which can satisfactorily reduce the ductile-to-brittle transition temperature of chromium.

2.3.3 Grain Size Effects

Observations of brittle fracture in chromium have found the origin of fracture to frequently be at the grain boundaries; suggesting a strong correlation between grain boundaries and premature failure. In 1963, Gilbert *et al.* found the DBTT of unalloyed, arc-melted chromium samples with impurity contents up to to 35 ppm C, 48 ppm O and 12 ppm N to be dramatically affected by the grain size of the material. This same research also found fine grained samples to have a DBTT of 90°C, and coarse-grained/mixed structures at ~30°C, further supporting the effects of grain size on the DBTT.[17] Correlating this with the findings of Hook et al., who discovered that single crystals of a similar purity were ductile to -78°C, suggests a correlation between crack initiation and the addition of grain boundaries.[17, 18]

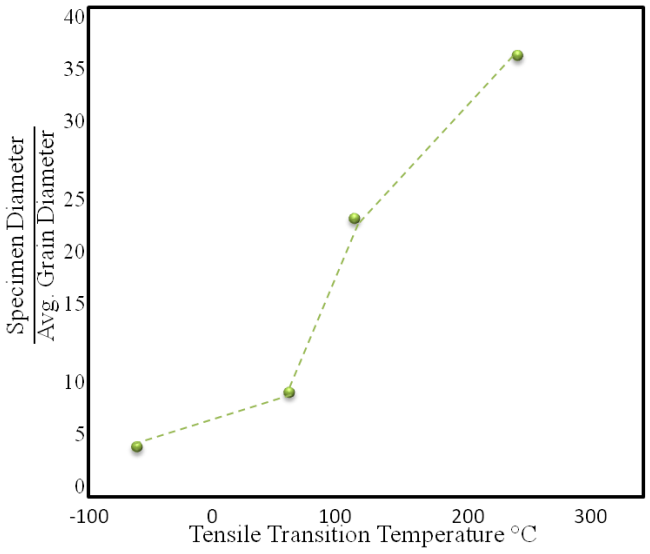

Figure 2.7: Effect of Grain Size on The Room-Temperature Yield Stress. Data Taken From Reference [16]

Figure 2.7 shows the relationship between grain size and transition temperature in unalloyed chromium.[16] From the figure it is concluded that fine grained chromium is more brittle than coarse grained (Figure 2.7). Hook et al. also observed that brittle fracture in chromium is primarily initiated from an intergranular rupture site, suggesting the controlling parameter is whether or not a microcrack can be initiated at the grain boundaries.[16] Therefore, by increasing the grain size or decreasing the number of grain boundaries, one can effectively decrease the number of potential intergranular rupture sites and subsequently decrease the DBTT.

2.3.4 Impurity Effects

Impurity effects on the transition temperature of chromium are largely dependent on the interstitial content and distribution.[19, 20] According to theoretical and experimental observations removal of nitrogen, oxygen, carbon and sulfur will result in sufficient ductility at low temperatures.[21] Nitrogen is the most detrimental of these impurities as concentrations of >.001wt% will embrittle pure chromium.[15, 22] The DBTT of as-cast chromium increases with increasing carbon content.[15, 23] A change in the fracture mechanisms of high carbon chromium are observed as they transition from cleavage fracture to intergranular fracture, suggesting the effect of carbon on the DBTT is through the formation of embrittling carbides at the grain boundaries.[15]

Preparation of high purity chromium can be challenging because of chromium's high melting point, high vapor pressure, and attraction to embrittling interstitals such as carbon, nitrogen, sulfur and oxygen.[24] Additionally, the high melting point eliminates ingot casting as a means of fabrication as containing the melt becomes a challenge. Instead, vacuum arc melting and powder metallurgy (PM) have been used as manufacturing techniques for the development of high-purity chromium alloys.[25]

Since ductility is strongly correlated to purity, purification of chromium is an obvious way to decrease the DBTT.[15] Briant *et al*. recently studied the effect of

both purity and grain boundaries on the DBTT. High purity single crystal samples manufactured in a carbon free environment were prepared using an advanced powder metallurgy process and finished with a forging process which produced an equiaxed grain structure.[25] Samples showed significant ductility in a *4-point* bend test at room temperature. After rolling, recrystallizing and retesting the samples, Briant concluded that if the purity levels in chromium can be maintained then room temperature ductility is possible.[26] It should be noted that during subsequent work the authors noted significant increases in carbon levels in the PM samples due to a graphite cylinder which was used for compaction.[25]

An apparent expedient for lowering the amount of interstitals present in commercially pure chromium is to add a scavenging element to stabilize or remove the interstitial impurities.[15] In 1963, Ryan experimented with many nitrogen and carbon scavengers in as-cast chromium. Elements Ce, La, Hf, Th, Ti, U, Y, Zr, where shown to react strongly during casting with N and C present, and to segregate those impurities.[21] Henderson *et al*. later confirmed these results and added that Nb and Ta were found to scavenge both N and O.[27] Nitride forming elements, Ce, Ti, Y and Zr were further studied in the 1960's and were proven later to promote room temperature ductility in recrystallized chromium.[22] Ideally, to minimize the effects of N and C, a combination of a strong carbide former and a strong nitride former must be used when lower grade chromium is used.

The effects that these impurities have on the ductility are thought to be through Cottrell locking of dislocations. In body-centered cubic materials any solute atom present will interact with its nearest neighbor by applying a small residual stress, all of which lie on planes of slip.[28] Impurities dissolved in the solid solution are believed to thwart dislocation motion by inhibiting slip and therefore preventing ductility. In chromium it has been found that nitrogen prevents dislocation movement by precipitation in dislocation lines.[28, 29] Additionally, in 1957 Wain et al. postulated that if Cottrell locking is responsible for room temperature brittleness in chromium that pre-deforming the sample in the plastic regime to

produce mobile dislocations should lower the DBTT.[29] Cottrell locking has never definitively been correlated to brittleness in chromium, yet pre-deforming chromium in the plastic regime has been shown to increase room temperature ductility.

2.3.5 Pre-Deformation Effects

Pre-deformation of chromium has been a proven means of reducing the DBTT. Pre-deformation introduced at a temperature above the DBTT produces mobile dislocations and eliminates microvoids. Pre-deformation can be applied using conventional methods or hydrostatic pressurization.[15]

Pre-deformation of chromium by equal channel angular extrusion (ECAE) above the ductile-to-brittle transition temperature (DBTT) provides the mobile dislocations needed for ductility.[30] In 2002, samples of recrystallized chromium with carbon concentrations of 51ppm, and nitrogen impurities of 19 ppm, were tested after pre-deforming ($\varepsilon > 3\%$) the material at 400°C. In a three-point-bend test samples obtained a bending angle of 10° before fracture.[30] While these samples showed considerable promise the authors did note the samples contained a large quantity of micro-cracks after plastic deformation. These cracks grew considerably and were obviously the source of failure of the material.[30]

By reducing the number of micro-voids present, multiple deformation, ie. cycling the material to the yield point and then removing the load and repeating, was discovered to significantly enhance the room temperature ductility.[31] This process is believed to work well through the removal of preexisting micro-voids concentrated in the grain boundaries of sintered chromium.[32] Micro-void regions will cause premature failure as they will deform more readily than the neighboring chromium crystals with large shear moduli.[32] In 2000, it was shown in tensile tests that the area fraction of micro-voids in the total intergranular rupture region of high purity sintered chromium tensile tests was a predominant factor for controlling the fracture, regardless of test conditions.[31]

2.3.6 Alloying Additions

Finally, it should be obvious that increasing ductility in chromium can be attained with the addition of alloying elements. Previous research has tried to correlate the mechanical properties of the alloying element with its effect on the DBTT. However, only the atomic size of the alloying element has been proven to strongly influence the DBTT.[33] In 1964, Carlson *et al*. concluded from his work on iodide chromium that alloying additions which form solid-solution alloys, and have an atomic diameter larger than chromium but not exceeding 15%, will lower the DBTT of chromium-based alloys.[33] More importantly they concluded that atoms with an atomic diameter 2-10% larger than chromium have the greatest impact on the DBTT.[33]

During the 1960's extensive research was done on the "rhenium ductilizing effect," which is a phenomenon originally observed in Cr-(25-35%)Re. Not specific to rhenium, it promotes room temperature ductility and twinning in group 6 based alloys. This effect has also been observed in chromium when alloyed with Groups 7,8,9 and 10 solutes.[34] In chromium some of the known rhenium analogs include: Fe, Ru and Co, while elements which partially resemble this effect include: Ti, V,Nb, Ta,Ni, Os, Ir. [35] In 1975, Klopp noted elements which were likely to exhibit this ductilizing effect, met the following criteria: [36]

1. Ductilizing solutes are from the groups 7,8,9,10 of the periodic table [15]
2. Maximum room-temperature ductility occurs in saturated or supersaturated single phase solid solution alloys [15]
3. Ductilizing solute must have a high solubility in chromium, in excess of 20% [34]
4. System must also contain an intermediate sigma-phase [34]

In 2008, Gao *et al.* determined that to improve ductility, an alloying addition must have a positive impact on Poisson's ratio while lowering the shear modulus as these are the two mechanical properties with the greatest impact on ductility.[37] It is generally accepted that Poisson ratio is a good indication of ductility in crystalline

and amorphous alloys, the higher the Poisson ratio, generally, the more ductile the material.[38] The shear modulus relates to ductility through the Rice Thompson Parameter (Equation 2.1), which describes the ease of dislocation motion through a crystalline material.[39]

$$\frac{\mu b}{\gamma} \qquad \text{Equation 2.1}$$

μ is the shear modulus, b is the Burger's vector and γ is the surface energy of the fracture plane.

To determine the effect of an alloying addition on the Poisson's ratio and the shear modulus of chromium, a series of first-principles density functional theory calculations were performed to predict the Poisson's ratio and shear modulus of various chromium binary alloys. Elements for the study were first selected based on their solubility in chromium up to high temperatures.[37] Bulk modulus, shear modulus, heat of mixing, atomic volume and Poisson's ratio were calculated for each alloy and 5 elements were predicted to have the most potential ductilizing effect on chromium: Ti, V, Zr, Nb, and Hf.[37]

Recently, Kurishita et. al. successfully fabricated a V-28Cr-2.3Y and V-52Cr-1.8Y which exhibited superior mechanical properties at room temperature. An advanced powder metallurgy process using mechanical alloying and hot isostatic pressing was employed to circumvent the embrittlement which can occur in these alloys during casting.[40] Yittrium was added to the alloy to consume O and N introduced by the vanadium and in the pressing process formed finely dispersed particles of Y_2O_3 and YN.[40] Results from the room temperature tensile tests of the two compositions with varying annealing temperatures and times found the V-28Cr-2.3Y to have a yield strength of 440-850MPa and a total elongation of 14-26% and V-52Cr-1.8Y to have a yield strength of 610-740MPa and a total elongation of 10-19%. [40] Finally, by cold rolling the specimens at 1200°C an increase in the %reduction in area from 57-64% was observed. With these results Kurishita concluded it was the advanced processing which produced the high purity matrix

free from O and N and the precipitation of the impurities at the grain boundaries that enabled the superior mechanical properties.[40]

Accrediting the advanced processing techniques with the reduction of impurities at the grain boundaries Kurshita achieved marked ductility. For the successful development of powder metallurgy chromium vanadium materials, further experimentation must be done to measure the effects of vanadium additions and processing on the mechanical properties. Therefore the focus of this research is to measure the effects of processing and vanadium content on the ductile to brittle transition temperature of chromium.

3. 0 Methods

3.1 Sample Preparation

Three different sources were used for obtaining high purity Chromium (99.99%), Vanadium (99.8%) and Yttrium (99.9%) powders; Atlantic Equipment Engineers, Noah Technologies Inc., and American Elements, respectively. Cr and V powders were -100 mesh and Y powder -325 mesh. Consolidation of powders was done at Bodycote. The four chemical compositions of the powder mixtures are listed in Table 3.1. Table 3.2 shows the impurity content of each composition which was verified according to ASTM standard E1019-03.[41]

Table 3.1: Atomic% Composition of Powder Metallurgy Samples

Sample	Cr	V	Y
R7	99.96%		.04%
R8	74.29%	25.40%	.31%
R9	48.92%	50.50%	.58%
R10	23.75%	75.40%	.85%

Table 3.2: Leco Analysis Results

Sample	Trial	C	S	N	O
R7	1	0.02	<.005	<.005	0.066
	2	0.03	<.005	<.005	0.077
	3	0.02	<.005	<.005	0.06
R8	1	0.06	<.005	<.005	0.15
	2	0.07	<.005	<.005	0.12
	3	0.05	<.005	<.005	0.14
R9	1	0.04	<.005	<.005	0.11
	2	0.05	<.005	0.03	0.21
	3	0.02	<.005	-	-
R10	1	0.22	<.005	<.005	0.036
	2	0.15	<.005	0.084	0.23

After mixing and canning the powders in low carbon steel samples were hot isostatically pressed (HIPed) at 1250°C (±15°C) and 103MPa (15 ksi) for 4 hours. After HIPping, samples were returned to National Energy Technology Laboratory, Albany, Oregon where the can material was removed by machining. Next, the

chemical compositions of the samples were verified by X-ray fluorescence (Table 3.3).

Table 3.3: Final Alloy Composition Determined by X-ray Fluorescence (wt%)

	R7	R8	R9	R10
Cr	*99.79*	*72.23*	*46.80*	*23.07*
V	*<0.010*	*27.35*	*52.55*	*76.05*
Y	*0.066*	*0.26*	*0.46*	*0.67*
Mn	<0.010	<0.010	<0.010	<0.010
Si	<0.010	<0.010	<0.010	<0.010
Ni	0.11	0.28	0.47	0.63
Co	<0.010	<0.010	<0.010	<0.010
Mo	<0.010	<0.010	<0.010	<0.010
W	0.027	0.063	0.10	0.14
Nb	<0.010	0.018	0.028	0.037
Ti	<0.010	<0.010	<0.010	<0.010
Al	0.048	0.022	0.020	0.036
Fe	<0.010	<0.010	<0.010	<0.010
P	<0.010	<0.010	<0.010	<0.010
Cu	<0.010	<0.010	<0.010	<0.010
Ta	<0.010	<0.010	<0.010	<0.010
Mg	0.015	0.024	<0.010	<0.010

Samples of R7, R8, R9 and R10 received homogenization heat treatments at 1300°C for times denotated in Table 3.4. Finally, the samples were extruded at 1200°C to an area reduction of 6:1 in a high strain rate extrusion press, at a punch to billet rate of 40 ft/s at Pittsburgh Materials Technology, Inc. after being canned in low carbon steel. To obtain straight rods the extruded pieces were heated to 1000°C then swaged. Finally, the can material from the extrusion was removed using machining and centerless grinding. The resulting rods were approximately 13mm in diameter.

Table 3.4: Time of Heat Treatments at 1300°C

Time Abbreviation	Hours
T1	0
T2	24
T3	48
T5	120
T6	120 hours + Extruded

Test specimens were obtained from the extruded rods using wire electro discharge machining (EDM) performed at Wright Prototype in Albany, Oregon.

3.2 Microstructure

3.2.1 Optical Microscopy and Grain Size Analysis

The comparative method of determining grain size was used to determine the grain size of all samples after extrusion in both the longitudinal and transverse directions in accordance with ASTM Standard E112-96. Samples were prepared using metallographic techniques; they were polished to 1200 grit using a series of SiC abrasive papers. Then a solution of 2 parts .05μm colloidal silica and 1 part, 5% NaOH, 1% $K_3Fe\ CN_6$ and 94% distilled water, was used as a final attack polish. Using a Leica DMR upright microscope, brightfield reflective light and a magnification of 100x samples were analyzed and the grain sizes recorded.

3.2.2 X-Ray Diffraction

Samples were prepared for X-ray diffraction (XRD) as described previously for optical microscopy. XRD was performed using a Rigaku Ultima III X-Ray Diffractometer with a copper source. Samples were analyzed at 40kV and 40mA from 5-115° (2-Theta), at a scan width of .01°and scan rate of .25°/min in a standard sample block. Accuracy of the diffractomer is ensured through weekly calibration using a quartz standard.

3.2.3 Microprobe Analysis

A diffusion analysis was performed to study the homogenization of chromium and vanadium alloys at 1300°C. The diffusivity (*D*) of Cr and V was calculated from concentration profiles obtained from a Cameca SX100 electron microprobe with 5 wavelength dispersive spectrometers. Scans were taken at 15kV accelerating voltage and 30nA probe current. Scans were done across grains at 1-2

micrometer step sizes for all compositions and heat treatments. Cast homogeneous standards of all four compositions were used to ensure the accuracy of the electron microprobe.

To calculate the diffusivity of Cr-V both Fick's Second Law and the least square method were used. Although diffusion in the samples occurs in three dimensions, a 1-D model was used to simplify the calculations. Equation 3.1shows Fick's second law as it applies to an "infinite" 1-dimensional system.[42]

$$C = \frac{C_1 + C_2}{2} - \frac{C_1 - C_2}{2} erf\left(\frac{x}{2\sqrt{Dt}}\right) \qquad \text{Equation 3.1}$$

C is the actual concentration of chromium using the microprobe data, C_1 and C_2 are the initial concentrations of chromium, x is the length step in cm, t is the time of homogenization in seconds, D is the diffusivity (cm^2/s). Equation 3.2 is the least squares equation and is used to calculate how well the calculated data fits the actual data points. When the error has been minimized the best equation which describes the data has been obtained.

$$\varepsilon = \sum_{i=1}^{n} (y_i - \hat{y}_i)^2 \qquad \text{Equation 3.2}$$

ε is the error to be minimized, n is the total number of length steps, i is the current length step, y_i is an experimental data point and $\hat{y}_i$ is a calculated data point. For these experiments D should be chosen so as to minimize the sum of the squares ε. Combining Equation 3. 1 and Equation 3. 2 then taking the derivative and setting it equal to zero, produces Equation 3.3.

$$\frac{\partial}{\partial D}\sum_{i=1}^{n} C_i - \left(\frac{C_1 + C_2}{2}\right) + \left(\frac{C_1 - C_2}{2}\right) \cdot erf\left(\frac{x_i}{2\sqrt{Dt}}\right) = 0 \qquad \text{Equation 3.3}$$

The concentration curves were fitted using Equation 3.3 and the resulting diffusivities calculated using Mathematica.

3.3 Mechanical Testing

3.3.1 Elevated Temperature Vickers Hardness

For the Cr-V alloys hot Vickers hardness testing was done to determine the temperature range over which the hardness of the specimen changes. Testing was done using a Marshall Hot Hardness Vacuum Testing System over a temperature range of 25°C to 900°C under high vacuum (~2.5×10^{-5} torr). Samples were first polished using a series of SiC papers to a final 1μm diamond slurry. Each sample was heated from room temperature to 900°C at 100°C intervals. After the sample was allowed to equilibrate for 10 minutes, three indentations at $1Kg_f$ were made at each temperature. Indentations were measured using a Buehler Micromet II Microhardness Tester at 40X magnification. Indentation diameters (d_0) were averaged and the Vickers Hardness calculated using Equation 3.4.[43]

$$\frac{1854.4 \cdot 1Kg_f}{d_0^{\,2}} \qquad \text{Equation 3.4}$$

Estimated values of yield strength were determined using Equation 3.5.[44]

$$\sigma_y = \frac{H_v}{3} \qquad \text{Equation 3.5}$$

Where σ_y is the estimated yield strength, and H_v is the Vickers hardness.

3.3.2 Elevated Temperature 3-Point *Bend*

3-point bend tests were performed in general accordance with ASTM Standard 1161-02c, in an Instron Servo Hydrolic Universal Tester, Model 8872, with an Applied Test Systems Environmental Chamber #3710. Samples were machined using wire electro discharge machining (EDM) to the configuration shown in Figure 3.1. Using a *3*-point bend fixture with a nominal roller diameter of 12.5 mm and a support span of 40 mm, testing was done at a strain rate of 10^{-3}/s or a crosshead speed of .571 mm/min, under a continuous flow of 30 cc/min of argon. The strain rate was calculated using Equation 3.6

$$\dot{\varepsilon} = \frac{6ts}{L^2}$$ Equation 3.6

Where $\dot{\varepsilon}$ is the strain rate (10^{-3}), t is the specimen thickness, L is the outer (support) span and s is the crosshead speed.

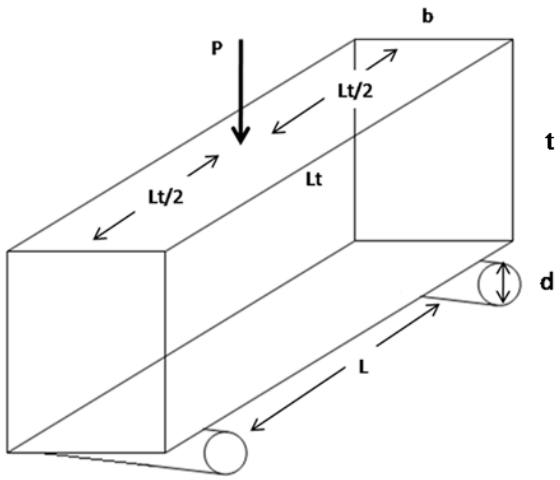

Figure 3.1: 3-point Bend Test Specimen Dimensions [45]

Table 3.5: Dimensions of *3-point* Bend Specimens

Dimensions, mm		
Length	L_t	45
Thickness	t	3.0
Width	b	4.0
Nominal Bearing Diameter	d	4.5
Support Span	L	40

2 sets of unalloyed Cr samples with different surface conditions were prepared to evaluate the notch sensitivity of Cr and its effects on the DBTT. The first sample set was prepared by electropolishing with a 10% perchloric acid in methanol solution at -30°C and an operating voltage of 15V. The second set was prepared using the attack polish procedure described previously. The attack polish used has been noted to attack vanadium more aggressively than chromium and therefore samples which did not receive an attack polish were also tested to measure the

effects of surface conditions. Samples in the non-attack polished condition were polished using SiC papers up to 1200 grit.

Strain values for large scale strain were calculated using the radius of curvature. It was assumed that the neutral axis does not change length and all parallel planes remain parallel. With these assumptions (Figure 3.2) an equation for true strain was derived.

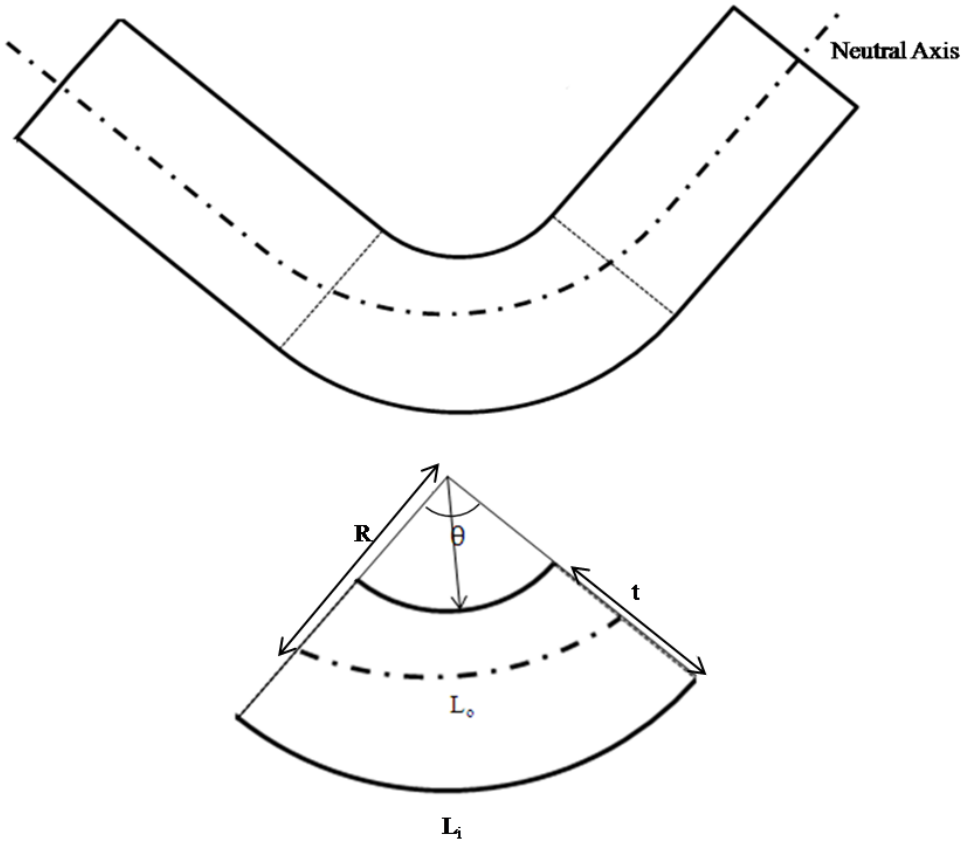

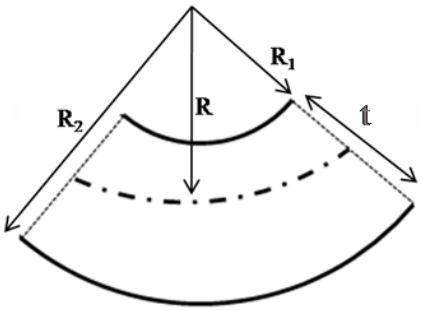

Figure 3.2: *3-point* Bend Beam Diagrams

Beginning with the equation for true strain (Equation 3.7) each strain value was correlated to the actual sample geometry.

$$\varepsilon_{true} = \ln\left(\frac{L_i}{L_0}\right) \qquad \text{Equation 3.7}$$

Plugging in the values for L_i and $L_{0,}$ Equation 3.8 provides the equation for true stain of curved beams.

$$\varepsilon_{true} = \ln\left(\frac{\theta\left(R+\frac{t}{2}\right)}{\theta(R)}\right) \qquad \text{Equation 3.8}$$

Where R is the radius of the neutral axis, t is the height of the sample, and θ is the angle of curvature. Next by canceling θ's and R the equation can be reduced to Equation 3.9.

$$\varepsilon_{true} = \ln\left(1+\frac{t}{2R}\right) \qquad \text{Equation 3.9}$$

Finally, by assuming R>>t the equation can be reduced to Equation 3.10.

$$\varepsilon_{true} = \frac{t}{2R} \qquad \text{Equation 3.10}$$

Adobe Photoshop was used to measure the radius R_1 and R_2 . A circle was drawn to match the curvature of radius R_1 and R_2, and corresponding pixel radius of the circles was recorded.

3.3.3 Elevated Temperature Tensile Test

Tensile specimens were obtained from the extruded rods using wire EDM performed at Wright Prototype in Albany, Oregon. Samples were prepared according to ASTM E8, and testing was performed in general accordance with ASTM E21. Dimensions and a drawing of test specimens are shown below in Table 3.6 and Figure 3.3. Tests were performed in an Instron Servo Hydrolic Universal Tester, Model 8872, with an Applied Test Systems Environmental Chamber #3710 under 30cc/min argon at a temperature range of 21°C-380°C.

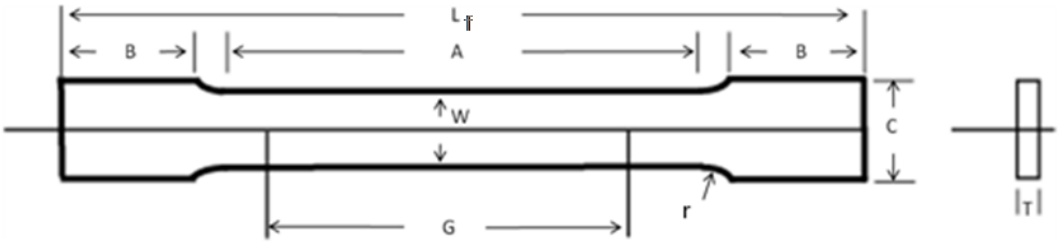

Figure 3.3: Tensile Specimen [46]

Table 3.6: Dimensions of Tensile Specimens

Dimensions, mm		
Length of Reduced section, min	A	30
Length of grip section, min	B	10
Width of grip section	C	10
Gage length	G	25.0 $\pm$ .1
Overall length, min	L_f	55
Radius of fillet, min	r	6
Thickness	T	3
Width	W	6.0 $\pm$ .1

3.3.4 Fracture Surface Analysis

Fracture surface analysis was performed on all elevated temperature *3-point* bend and elevated temperature tensile specimens using a combination of energy dispersive spectroscopy (EDS) and scanning electron microscopy (SEM). Two SEMs were used for the analysis an FEI Quanta 600 FEG with an EDAX EDS detector and an FEI

Inspect F with an Oxford EDS detector. Operating voltage of 20kV was used with a 5.0 micron spot size at various magnifications to locate critical fracture features. Samples were mounted to a standard sample block and secured using carbon tape. Additionally, the tensile, compressive and unstressed regions of 3-point bend specimens were analyzed to locate any surface damage which may have impacted test results.

3.3.5 Stress Intensity Factor Calculations

Using cracks measured at the unstressed end of the beam and the K_1 equation developed by Newman and Raju (Equation 3.11) an estimation of the stress intensity factor (K_1) of 50Cr-50V was calculated.[47]

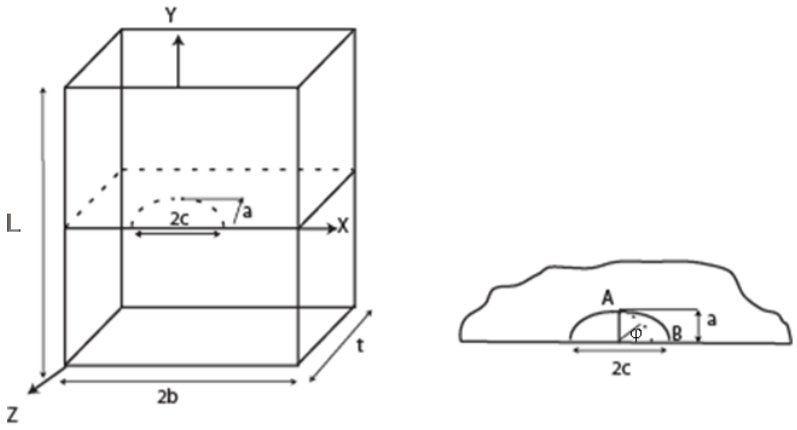

Figure 3.4 Surface Crack in a Finite Plate. Taken From Reference [47]

$$K_1 = (S_t + HS_b)\sqrt{\pi \frac{a}{Q}} F\left(\frac{a}{t}, \frac{a}{c}, \frac{c}{b}, \phi\right) \qquad \text{Equation 3.11}$$

For $0< a/c < 1.0$, $0 < a/t < 1.0$, $c/b < .5$ and $0 < \phi < \pi$ where K_1 is the stress intensity factor, S_t is the remote uniform stress (tension), S_b is the remote uniform stress (bending), *a* is the depth of the surface crack, t is the plate thickness, *b* is the half-width of the crack plate, *c* is the half-length of the surface crack and ϕ is the

parametric angle of the ellipse in degrees (Figure 3.4). *Q*, *H*, and *F* are given in Equations 3.12, 3.19 and 3.13.

$$Q = 1 + 1.464\left(\frac{a}{c}\right)^{1.65} \quad \left(\frac{a}{c} \leq 1\right) \qquad \text{Equation 3.12}$$

Q is the shape factor for an elliptical crack. F is defined so that the boundary correction factor for tension is equal to F and the boundary correction factor for bending is equal to the product of F and H. F is given in Equation 3.13 and H is defined in Equation 3.19.

$$F = \left[M_1 + M_2\left(\frac{a}{t}\right)^2 + M_3\left(\frac{a}{t}\right)^4\right] f_\phi g f_w \qquad \text{Equation 3.13}$$

Where

$$M_1 = 1.13 - .09\left(\frac{a}{c}\right) \qquad \text{Equation 3.14}$$

$$M_2 = -.54 + \left(\frac{0.89}{0.2+\left(\frac{a}{c}\right)}\right) \qquad \text{Equation 3.15}$$

$$M_3 = 0.5 - \frac{1.0}{0.65+\left(\frac{a}{c}\right)} + 14\left(1.0 - \frac{a}{c}\right)^{24} \qquad \text{Equation 3.16}$$

$$g = 1 + \left[0.1 + 0.35\left(\frac{a}{t}\right)^2\right](1 - \sin\phi)^2 \qquad \text{Equation 3.17}$$

$$f_\phi = \left[\left(\frac{a}{c}\right)^2 \cos^2\phi + \sin^2\phi\right]^{\frac{1}{4}} \qquad \text{Equation 3.18}$$

f_ϕ is an angular function from the embedded elliptical crack solution. f_w is a finite-width correction (Equation 3.18).

$$f_w = \left[\sec\left(\frac{\pi c}{2b}\sqrt{\frac{a}{t}}\right)\right]^{1/2} \qquad \text{Equation 3.18}$$

H is defined as a component of the boundary correction factor for bending and is given in Equation 3.19.

$$H = H_1 + (H_2 - H_1 \sin^{\mathrm{P}} \phi) \qquad \text{Equation 3.19}$$

$$p = .02 + \frac{a}{c} + 0.6\frac{a}{t} \qquad \text{Equation 3.20}$$

$$H_1 = 1 - 0.34\frac{a}{t} - 0.11\frac{a}{c}\left(\frac{a}{t}\right) \qquad \text{Equation 3.21}$$

$$H_2 = 1 + G_1\left(\frac{a}{t}\right) + G_2\left(\frac{a}{t}\right)^2 \qquad \text{Equation 3.22}$$

$$G_1 = -1.22 - 0.12\frac{a}{c} \qquad \text{Equation 3.23}$$

$$G_2 = 0.55 - 1.05\left(\frac{a}{c}\right)^{0.75} + 0.47\left(\frac{a}{c}\right)^{1.5} \qquad \text{Equation 3.24}$$

4.0 Results

4.1 Microstructure

4.1.1 Optical Microscopy and Grain Size Analysis

Figure 4.1 shows the microstructure of Cr-V samples after 120 hour heat treatment. All images were taken at 100X using differential interference contrast (DIC). It is noted that the 100Cr sample has a much larger grain size than the other samples. The black spots are porosity and the larger second phases are yittria. Also the 25Cr-75V and 75Cr-25V samples appear to have two significantly different grain sizes and an average grain size is given in Table 4.1. Results from the grain size analysis are provided in Table 4.1 and Table 4.2.

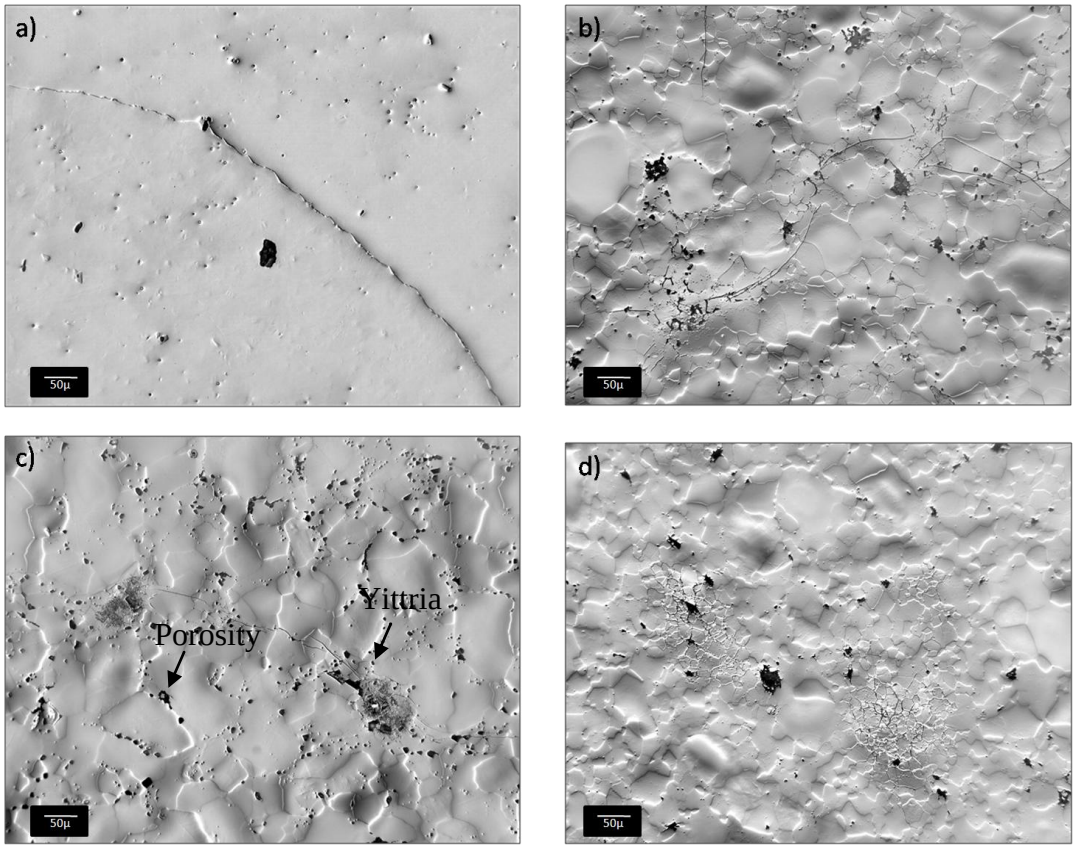

Figure 4.1: Optical Microscopy Showing Microstructure of 120 hr Heat Treated Samples a) 100Cr b) 50Cr-50V c) 75Cr-25V d) 25Cr- 75V

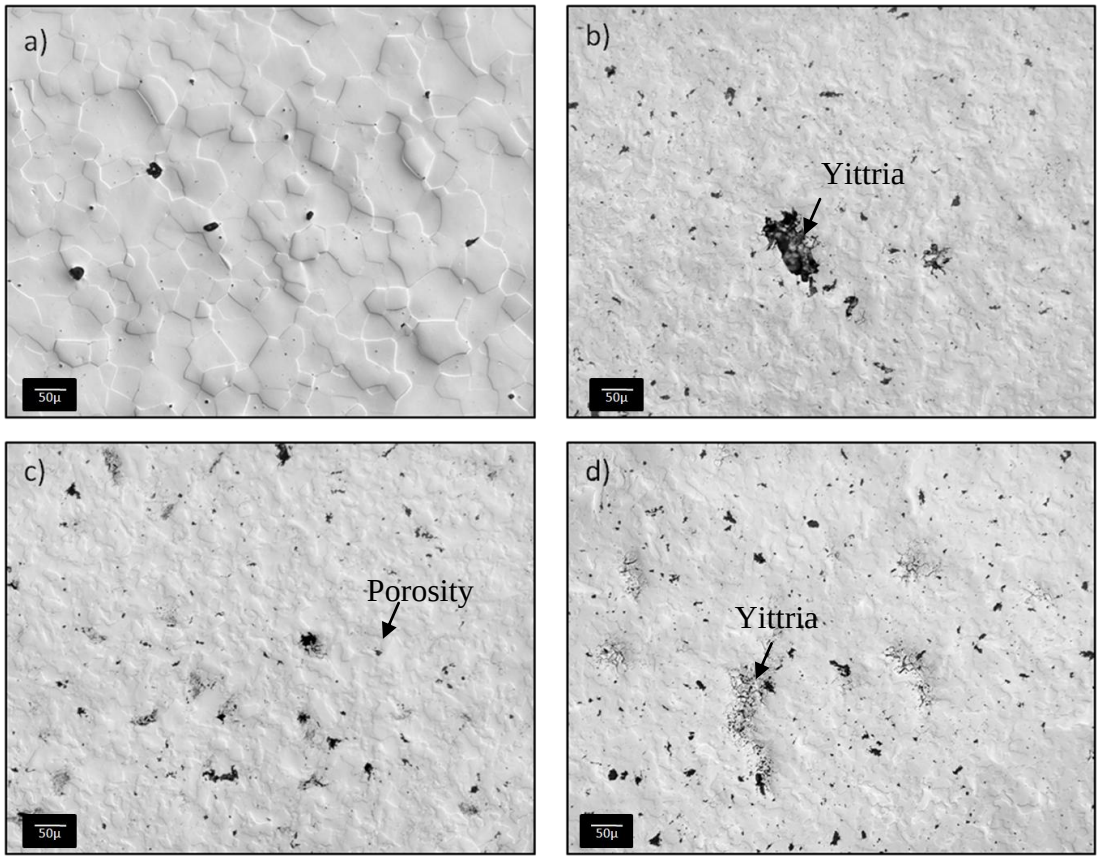

Figure 4.2: Optical Microscopy Showing The Transverse Direction of Extruded Samples Images Taken at 100X a) 100Cr b) 50Cr-50V c) 75Cr-25V d) 25Cr- 75V

In Figure 4.2 the microstructure of the extruded samples can be seen. As can be seen by comparing Figure 4.1 and Figure 4.2, extrusion of the samples had a significant impact in reducing the grain size, as quantified in Tables 4.1 and 4.2. It is noted the 100-Cr sample still has a larger grain size than any of the Cr-V samples. All of the Cr-V samples appear to have a similar microstructure and grain sizes. The porosity of the samples has also been reduced during extrusion as is evident by the reduction in the number of black spots.

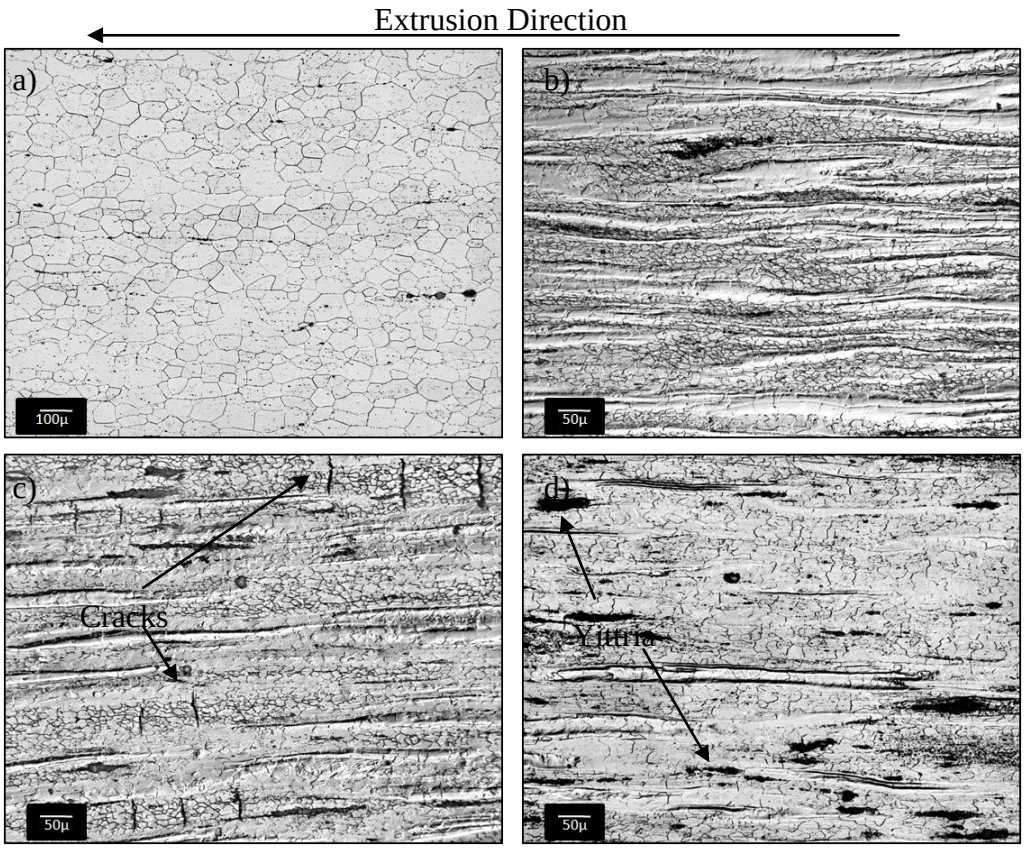

Figure 4.3:Optical Microscopy Showing the Longitudinal Direction of Extruded Samples a)100Cr (200X) b)75Cr-25V (100X) c)50Cr-50V (100X) d)25Cr-75V(100X)

Small grains in 75Cr-25V, 50Cr-50V and 25Cr-75V can be observed in the micrograph. Black spots observed in the samples are likely yittria on the surface as extrusion significantly reduced the number of pores in the sample. 100Cr appears to have a uniform grain size with little elongation as the grain size of the longitudinal and transverse orientations are roughly the same. This suggests recrystallization, as there was a grain size reduction in the 100Cr after extrusion. Cracks on the surface of the 50Cr-50V appear in uniform columns oriented parallel to the extrusion direction, with the individual cracks oriented perpendicular to the extrusion direction.

Table 4.1: Mean Grain Diameter of Cr-V Samples After 120 Hour Heat Treatment

Sample Number	Orientation	Magnification	ASTM Grain Size	Grain Diameter (μm)
R7-T5	Transverse	100	>1	>287
R8-T5	Transverse	100	5	67
R9-T5	Transverse	100	6	45
R10-T5	Transverse	100	7	32

Table 4.2: Mean Grain Diameter of Cr-V Samples After Extrusion

Sample Number	Orientation	Magnification	ASTM Grain Size	Grain Diameter (μm)
R7-T6	Transverse	100	5	67
R7-T6	Longitudinal	100	5	67
R8-T6	Transverse	100	9 ½	15-11.2
R8-T6	Longitudinal	100	9 ½	15-11.2
R9-T6	Transverse	100	9	13
R9-T6	Longitudinal	100	9	13
R10-T6	Transverse	100	9	13
R10-T6	Longitudinal	100	8	23

4.1.2 X-Ray Diffraction

X-ray diffraction data showing the effects of processing on the composition and structure of Cr-V alloys is found in Figure 4.4. The 2θ peaks of chromium and vanadium in the [110] plane can be found at 44.5° and 42° respectively.

100-Cr peaks shows no change in composition or structure with heat treatments as the Cr peak stays centered around 44.5° for all conditions.

Looking at the 0hr treatments in the 75Cr-25V, both the Cr and V peaks can be seen. At 24 hours the vanadium peak is more pronounced and has shifted towards the chromium peak indicating diffusion is occurring. After the longer heat treatment times as the two peaks shift towards each other until the only the solid solution peak is observed after the extrusion treatment.

In the 50Cr-50V at 0 and 24 hours both the vanadium and chromium peaks are discernable and of similar intensities. As diffusion takes place and a solid solution forms the two peaks converge to ~43° as seen for 50Cr-50V in the as-cast

condition where the solid solution peak is located. At intermediate heat treating times the location of Cr and V peaks are shifted towards each other indicating an increased degree of homogeneity.

For 25Cr-75V a small Cr peak is observed with a large V peak in the 0hours condition. At 24 hours the intensity of the Cr peak has diminished and the V peak has shifted slightly ~.5°. At 48 and 120hours the Cr peak disappears and only two solid solution Cr-V peaks remain

In the 50Cr-50V and 25Cr-75V samples in the extruded condition a broadening of the x-ray peak is observed. There are two observations which could account for this broadening. First, localized composition variances in the sample may have produced the broadening in the x-ray data. The broadening of the peaks is the result of many x-ray peaks centered at their respective compositions. Second, rather than converging towards the solid solution diffraction line, the extrusion process may have produced a non-uniform strain field observed as a broadening of the diffraction line. The effect of this strain field is small regions within a grain where the d spacing is substantially constant but different from the spacing in a neighboring region due to localized microstrains. The different spacing in each region within the grains causes many sharp diffraction peaks the sum of which is a broadened diffraction line for the extruded condition.

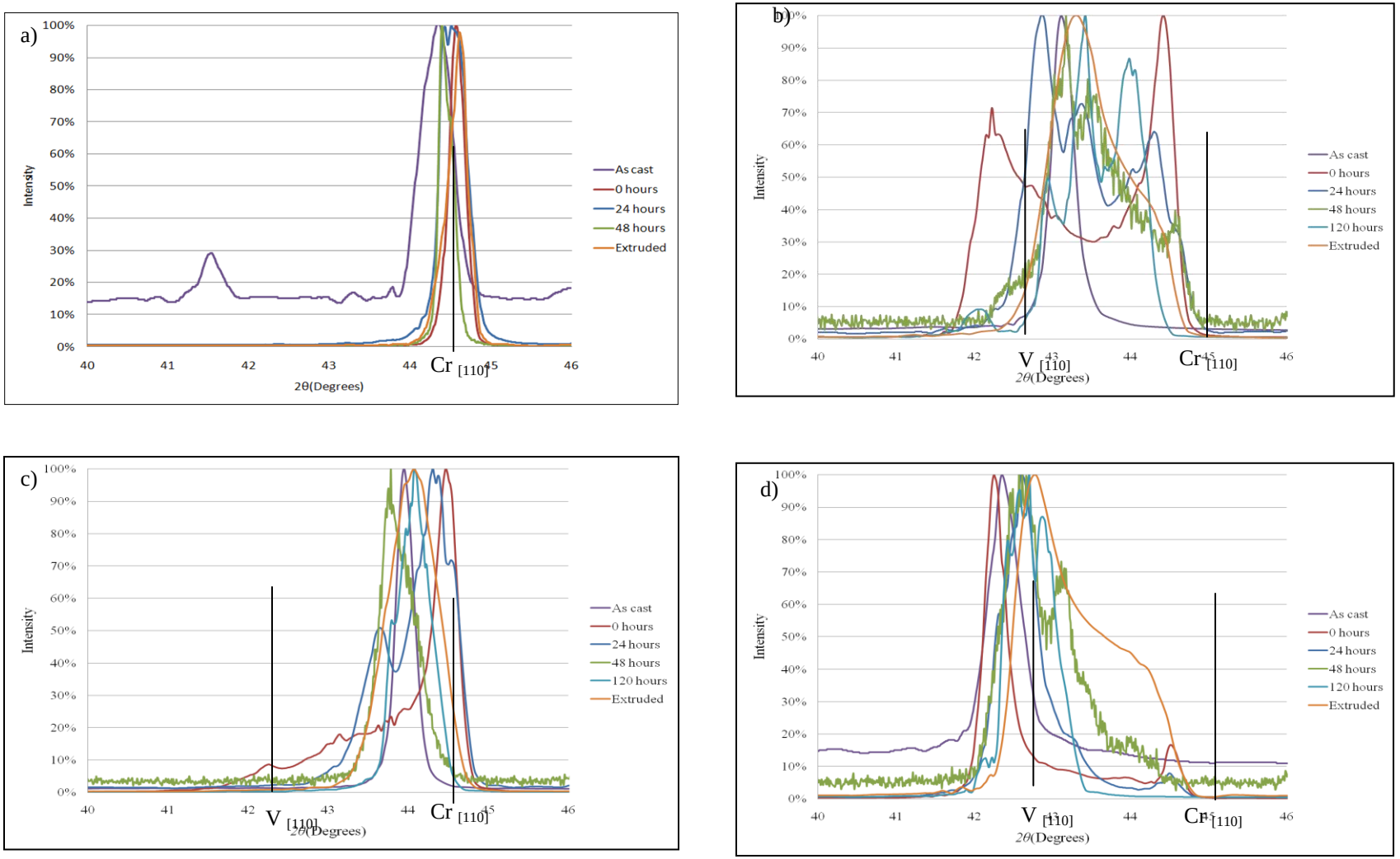

Figure 4.4: X-Ray Diffraction Results as a Function of Processing History a) 100-Cr b) 50Cr-50V c) 75Cr-25V d) 25Cr-75V

4.1.3 Microprobe Analysis

Figure 4.5 shows concentration gradient versus position data for as-HIPed 50Cr-50V obtained from the electron microprobe. This scan was taken from the center of one Cr grain to the center of a V grain. From this figure it is observed that not much diffusion has occurred during hot isostatic pressing. A change in the concentration profile is observed in the 20 micrometer region nearest the grain boundary. The concentration profiles can also be used as a rough estimation of the grain size of the samples. As can be seen in Figure 4.5 this Cr grain is approximately 80 micrometers in diameter.

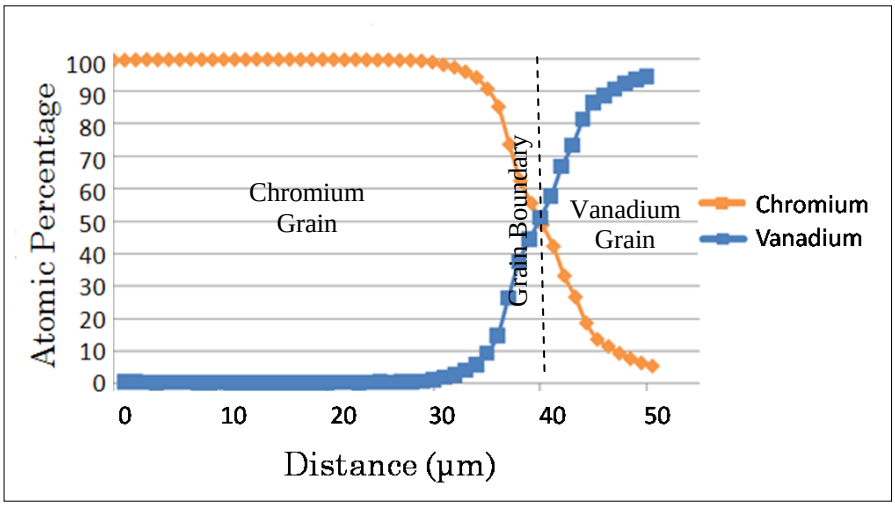

Figure 4.5: 50Cr-50V As-Hot Isostatically Pressed Concentration Vs. Position Profile taken at 1.0 µm Step-Size

Figure 4.6 shows the concentration profile of the 50Cr-50V sample after 1300°C and 120 hour heat treatment. As can be seen in the figure diffusion has occurred completely across the grains, as there is no region with 100 at% Cr or V. However, a region of ~95% chromium is observed suggesting further heat treating is required for better homogenity. There also appears to be some variability in the grain size as the vanadium grains appear to have diameters of 50 micrometers and 100 micrometers. The diffusion of Cr into V appears to be quite slow; therefore, grain refinement through extrusion was performed to reduce the grain size and increase mixing.

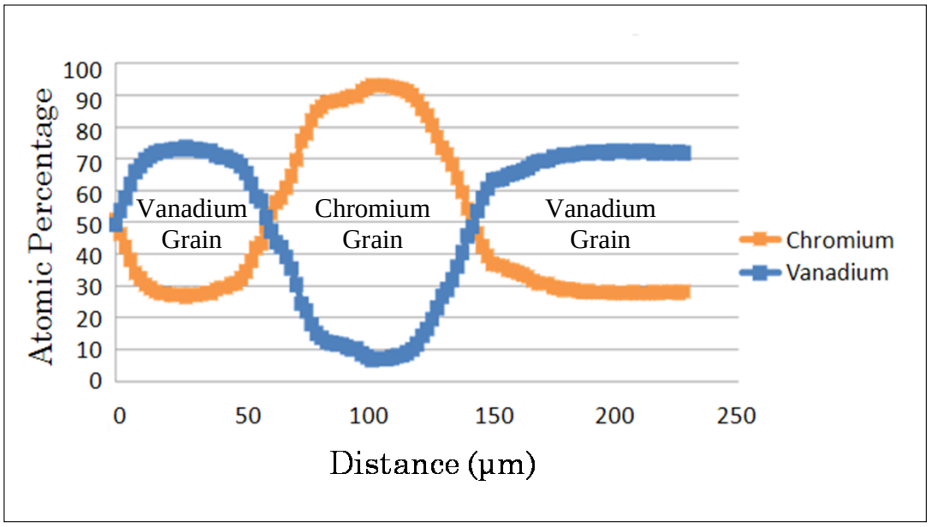

Figure 4.6: 50Cr-50V After 120 Hours 1300°C Heat Treatment Sample Concentration vs. Position Profile taken at 2.0 µm Step-Size

The effect of the extrusion process on the composition of the 50Cr-50V sample can be seen in Figure 4.7. The extruding process appears to have significantly reduced the size of the grains from ~50-100 micrometers to 5-15 micrometers. Extrusion also appears to have considerably increased the homogeneity of the sample, as only a small region (~5 micrometers) has a large chromium concentration (>90%).

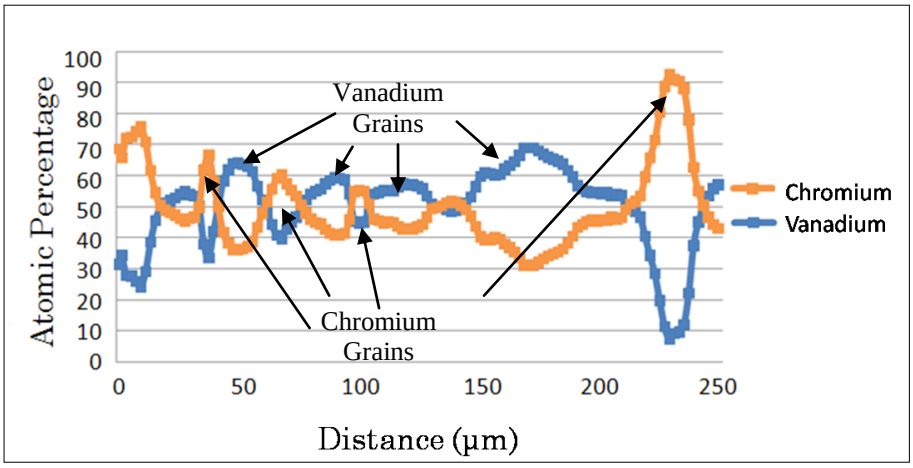

Figure 4.7: 50Cr-50V Extruded Sample Concentration vs. Position Profile taken at 2.0 µm Step-Size

Comparing Figures 4.5, 4.6 and 4.7 the effects of heat-treating and extrusion can be seen as the concentration profiles of the samples move towards 50 at% Cr and 50 at% V with heat treating and extrusion.

A calculated diffusivity obtained by curve-fitting was used for determining the heat treating and processing requirements of these samples. Using a combination of the Least Squares Method and Fick's Second Law a Mathematica code was created for each set of data. The calculated diffusivities for chromium into vanadium are given in Table 4.3. A factor of two variability is seen in the data and is assumed to be error correlated to the 1-D assumption made in the model. Compared to published diffusivity values of $2.4 \times 10^{-12} \frac{cm^2}{s}$ at 1200°C these diffusivities are considered to be in good agreement.[48]

Table 4.3: Calculated Diffusivities for Cr into V at 1300°C

Calculated Diffusivities (cm^2/s)
3.9E-11
3.90E-11
8.00E-12
1.30E-11
7.80E-12
2.40E-11
Average 2.18E-11
Standard Deviation 1.46E-11

A comparison of the best fit and actual concentration profile was used to evaluate the accuracy of the calculations and can be seen in Figure 4.8. There is good agreement between the fitted and observed diffusion rates as the difference between actual and calculated only varies by a few at% along the line.

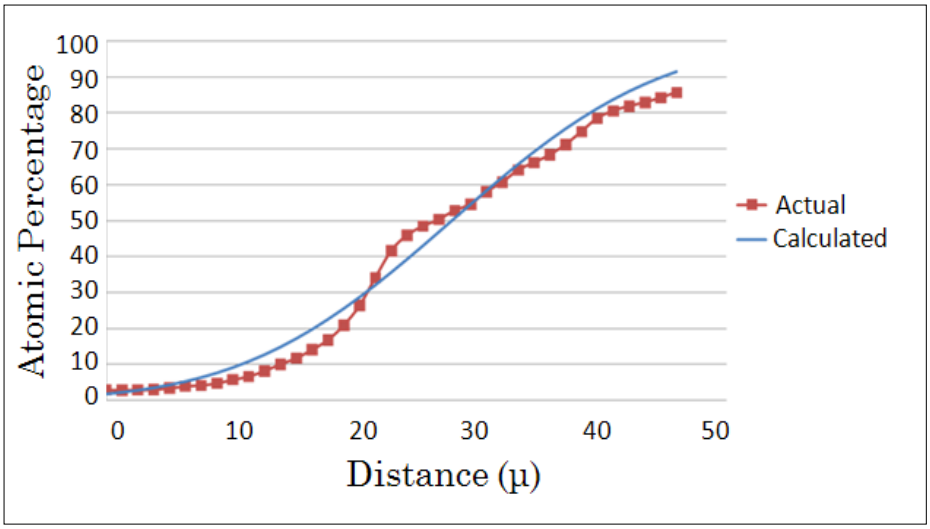

Figure 4.8: Calculated Concentration Profile Compared to Actual Concentration Profile

Finally the accuracy and precision of the electron microprobe (Table 4.4) was evaluated using cast Cr-V samples of known compositions. The results are considered to be both accurate and precise to a standard deviation < 1wt%, a range of < 2.5 wt%, and error of < 2%.

Table 4.4: Summary Statistics of the Accuracy and Precision of Electron Microprobe

Standard	Size of Sample (n)	Average Wt% Cr	Standard Deviation (σ)	Range	Average Wt% V	Standard Deviation (σ)	Range
25% Cr 75% V	19	25.579	0.2931	1.36	73.322	0.5960	2.014
50%Cr 50% V	27	50.201	0.4691	1.76	49.327	0.4765	1.840
75%r 25%V	24	75.594	0.7604	3.11	24.93	0.3378	1.160

4.2 Mechanical Testing

4.2.1 Elevated Temperature Vickers Hardness

Results from elevated temperature Vickers hardness testing are presented in Table 4.5,Table 4.6 , and Figure 4.9. As can be seen from the results there is an increase in the hardness of the samples with increasing vanadium content up to 50% after which hardness declines. Extruded samples also saw an increase in the hardness, presumably due to a refined grain size and increased homogeneity. Extrusion appears to have had the largest impact on the samples with the highest chromium content as 100Cr and 75Cr-25V samples achieved a ~50% increase in hardness. Looking at the hardness versus temperature, hardness of the samples is inversely related to the temperature. There also appears to be a change in the slope of the hardness trend of the heat treated and extruded samples around 300°C. This behavior is not conclusive evidence but may correspond to a transition in the brittle/ductile behavior.

Table 4.5: Elevated Temperature (25°C -900°C) Vickers Hardness (GPa) Values for 120 Hour 1300°C Heat Treated (T5) Samples, (Standard Deviation)

	Temperature (C°)							
	25	300	400	500	600	700	800	900
R7-T5	1.06 (.031)	0.59 (.046)	0.55 (.034)	0.50 (.033)	0.42 (.047)	0.47 (.034)	0.47 (.023)	0.35 (.018)
R8-T5	2.69 (.038)	1.47 (.011)	1.23 (.11)	1.15 (.040)	1.07 (.029)	1.13 (.039)	1.13 (.033)	1.20 (.009)
R9-T5	2.77 (.150)	2.46 (.619)	2.73 (.220)	2.04 (.364)	1.75 (.206)	1.89 (.415)	1.92 (.195)	1.84 (.356)
R10-T5	2.94 (.186)	1.65 (.067)	2.02 (.045)	1.65 (.108)	1.44 (.242)	1.51 (.223)	1.17 (.107)	0.90 (.122)

Table 4.6: Elevated Temperature (25°C -900°C) Vickers Hardness (GPa) for Extruded (T6) Samples, (Standard Deviation)

	Temperature (C°)							
	25	300	400	500	600	700	800	900
R7-T6	1.45	1.05	0.99	0.99	1.06	0.85	0.77	0.55
	(.077)	(.071)	(.069)	(.028)	(.035)	(.057)	(.006)	(.046)
R8-T6	3.13	2.47	2.11	1.83	1.85	1.81	1.78	1.43
	(.155)	(.300)	(.115)	(.105)	(.137)	(.112)	(.201)	(.040)
R9-T6	3.15	2.51	2.3	2.31	2.32	2.11	2.15	1.68
	(.076)	(.039)	(.051)	(.080)	(.147)	(.149)	(.170)	(.110)
R10-T6	2.87	2.31	2.18	2.19	2.03	1.86	1.53	1.15
	(.186)	(.082)	(.119)	(.095)	(.131)	(.131)	(.020)	(.054)

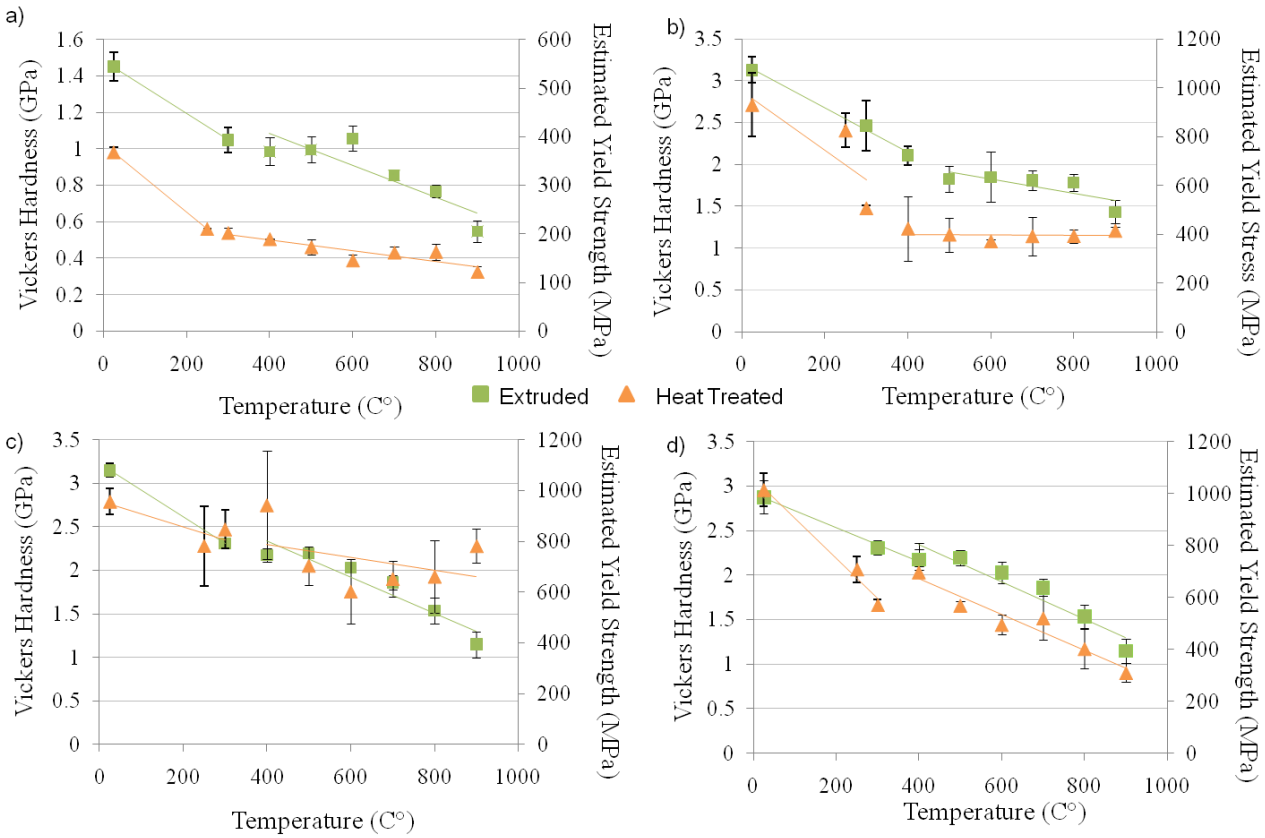

Figure 4.9: Vickers Hardness Versus Temperature With Linear Regression Fit a) 100-Cr b) 75Cr-25V c) 50Cr-50V d) 25Cr-75

4.2.2 Elevated Temperature 3-Point Bend Testing

Critical to the development of Cr-based alloys was to determine the effect of surface conditions on mechanical test results. As noted previously, samples of 100-Cr were prepared by attack polish and electropolishing. Figure 4.10 shows the elevated temperature *3-point* bend results for electropolished chromium devoid of mechanical polishing damage. A summary of the results can be found on Table 4.7. As can be seen from the table, 100-Cr exhibits substantial ductility at 380°C, achieving a flexure strain >20%. It should be noted this sample did not fracture, and testing was stopped once a bend angle ~ 45° was reached. Both the 80°C and the 180°C sample also seem to exhibit some ductility, as both samples achieved strain values > 6%. As to be expected the 26°C sample showed no ductility and fractured before 5% flexure strain was achieved.

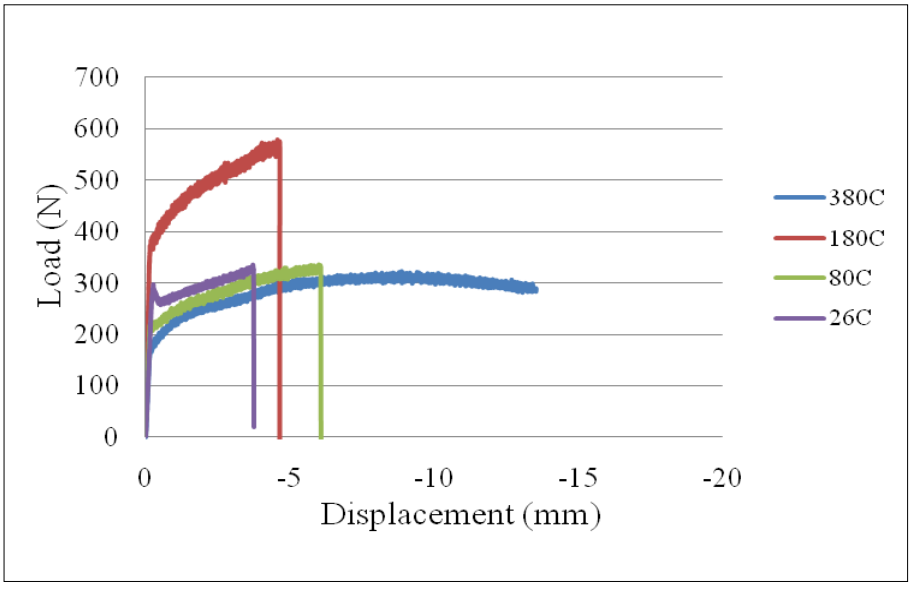

Figure 4.10: Load vs. Displacement in Electropolished 100Cr

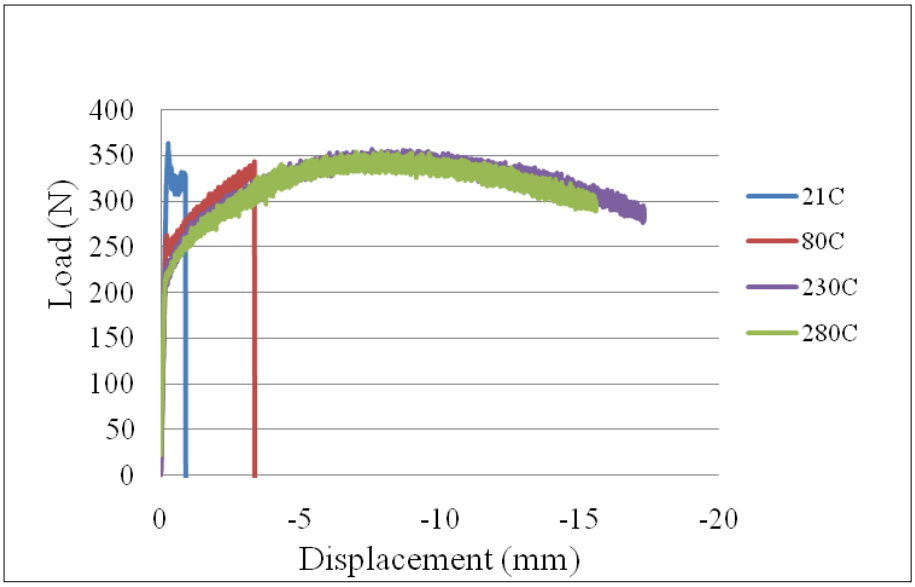

Figure 4.11: Load vs. Displacement Mechanically Polished 100Cr

In Figure 4.11 it can be seen that mechanically polished 100Cr exhibits exceptional ductility at 280°C and 230°C, achieving strain rates >20%. At 21°C and 80°C the samples behave similar to the 26°C electropolished samples. It is important to note that the surface conditions that were used in this test for pure chromium seem to have a negligible effect on the bend transition temperature of pure chromium, which appears to occur around 200°C based on Table 4.7.

Table 4.7: Summary of Results for 100-Cr Elevated Temperature *3-point* Bend Tests

Sample Number	Strain (mm/mm)	Max P (N)	σ_y (MPa)
R7-T6-EP-380C	>.22	315	248.8
R7-T6-EP-180C	.06	292	376.3
R7-T6-EP-80C	.08	327	404.9
R7-T6-EP-26C	.04	331	515
R7-T6-MP-230C	>.21	352	375.7
R7-T6-MP-280C	>.19	332	391.9
R7-T6-MP-80C	.04	336	405.3
R7-T6-MP-21C	.01	331	541.4

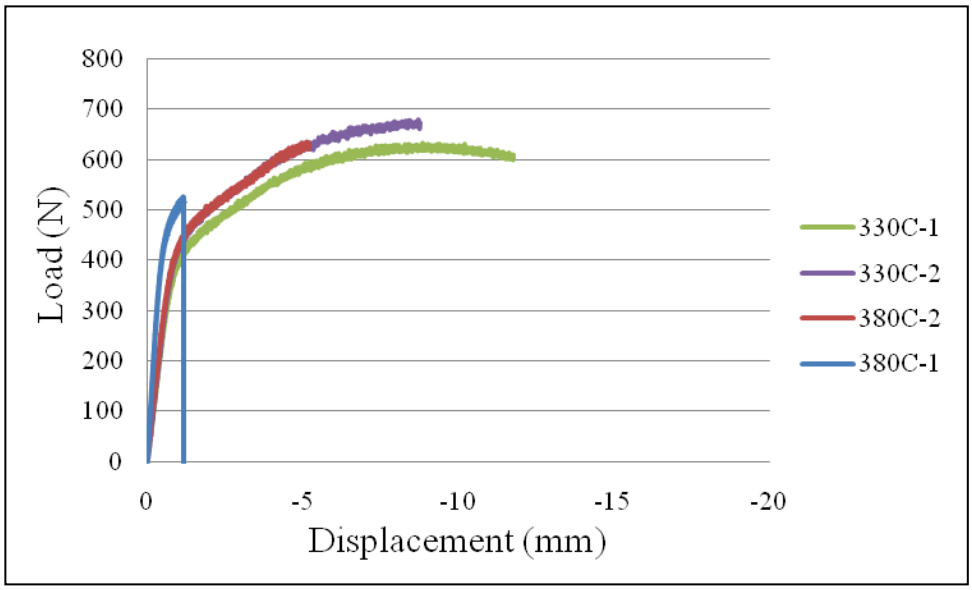

Figure 4.12: Load vs. Displacement 75Cr-25V

Figure 4.12 shows the *3-point* bend data for 75Cr-25V samples. As can be seen from the figure no obvious trend of temperature versus ductility is observed. Samples of both 380°C and 330°C exhibited both ductile and brittle behavior. With variability in yield strength of 874MPa-906 MPa and no observable plastic deformation at 380°C and large plastic regimes at 330°C the bend data does not seem to exhibit any obvious dependence of mechanical behavior on temperature.

Table 4.8: Summary of Results for 75Cr-25V Elevated Temperature *3-point* Bend Tests

Sample Number	Strain (mm/mm)	Max P (N)	σ_y (MPa)
R8-T6-380C-1	0.012	516	906.9
R8-T6-380C-2	0.052	633	874.0
R8-T6-330C-1	0.116	630	866.9
R8-T6-330C-2	0.09	677	875.3

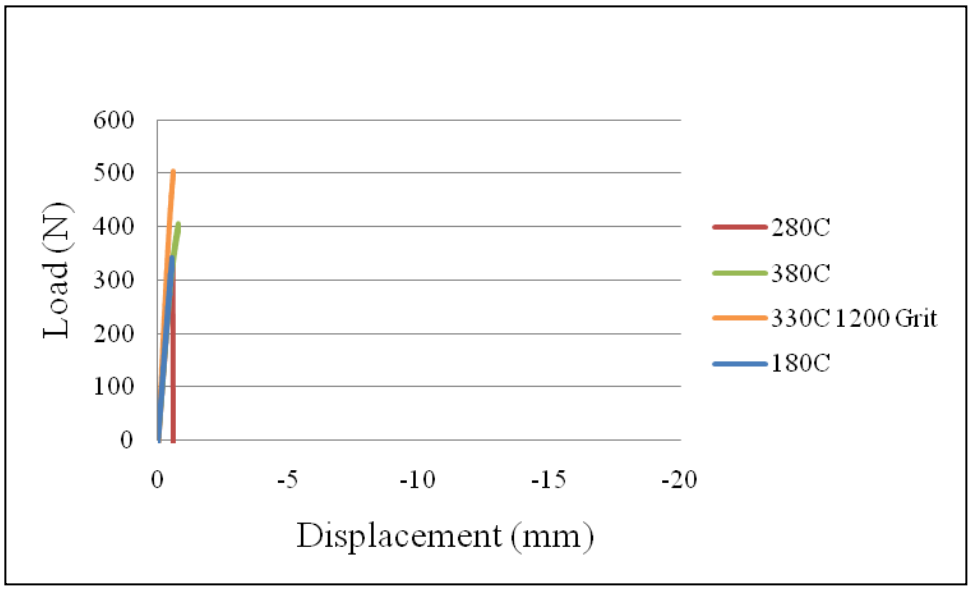

Figure 4.13: Load vs. Displacement 50Cr-50V

All samples of 50Cr-50V showed brittle behavior, as no specimen exhibited plastic deformation at any temperature. This brittle behavior is unexpected as both the 25%V and 75%V compositions showed measureable ductility at least at one temperature. To determine a relationship between surface conditions and mechanical behavior a specimen which did not receive an attack polish (330C-NP) was tested and performed similar to other specimens with only .7% strain achieved at 330°C. However, these specimens do show a weak relationship between temperature and failure strain and the specimens tested at the highest temperatures achieved slightly higher load values before failure.

Table 4.9: Summary of Results for 50Cr-50V Elevated Temperature *3-point* Bend Tests

Sample Number	Strain (mm/mm)	Max P (N)	σ_y (MPa)
R9-T6-380C	.008	405	478
R9-T6-280C	.005	338	525
R9-T6-180C	.005	336	852
R9-T6-330C-NP	.007	505	-

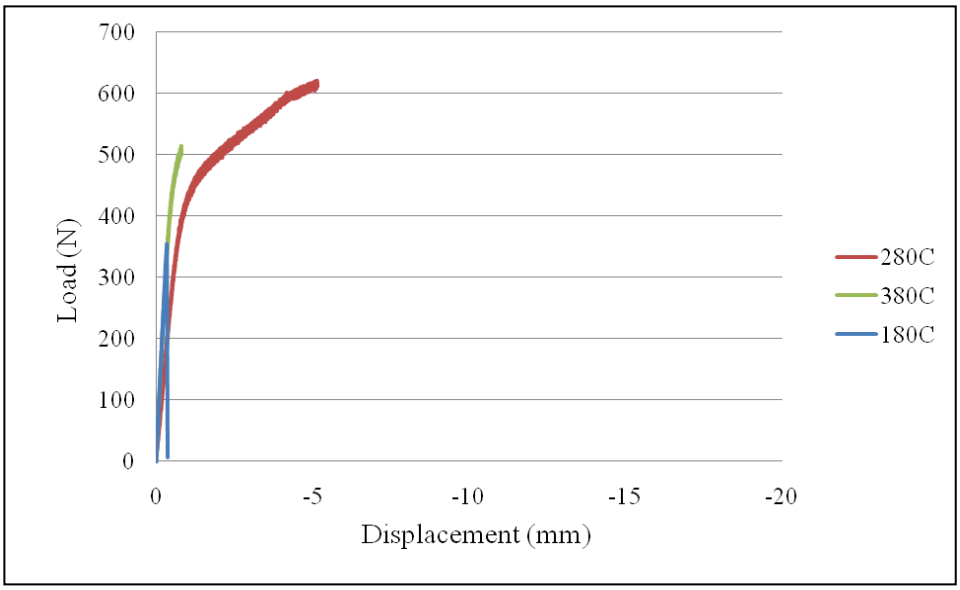

Figure 4.14: Load vs. Displacement 25Cr-75V

For 25Cr-75V as can be seen from the Figure 4.14 and Table 4.10 there is a difference between the failure stresses and strains of all samples, with the highest strain values achieved by the intermediate temperature. The peak load values and yield stresses are variable at all temperatures, as shown in Table 4.10. With less than 1% strain achieved in the 380°C and 180°C samples and 5.8% in the 280°C sample no trend in temperature affecting strain can be identified.

Table 4.10: Summary of Results for 25Cr-75V Elevated Temperature *3-point* Bend Tests

Sample Number	Strain (mm/mm)	Max P (N)	σ_y (MPa)
R10-T6-1-180C	0.003	355	304.2
R10-T6-2-280C	0.052	622	864.5
R10-T6-3-380C	0.008	516	918.4

4.2.3 Elevated Temperature Tensile Testing

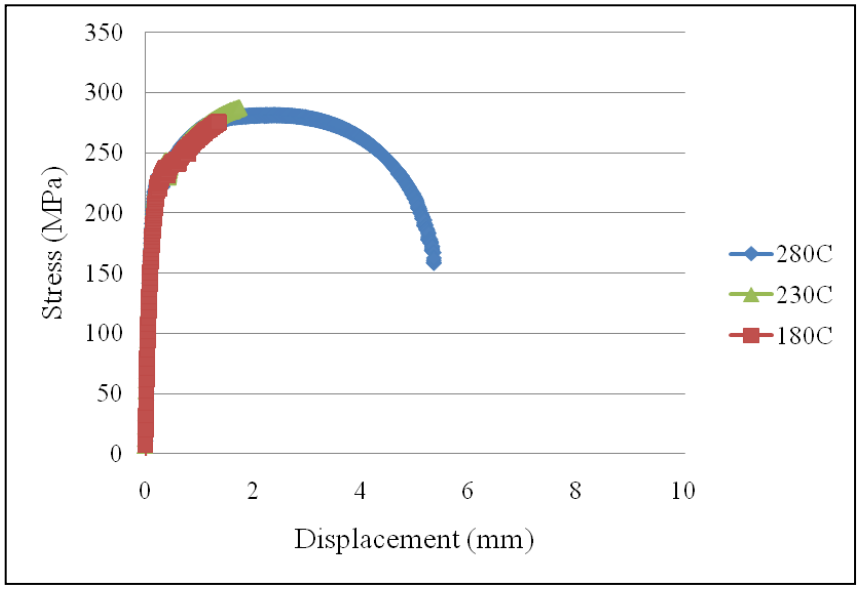

Figure 4.15: Elevated Temperature Tensile Results 100-Cr

The elevated temperature tensile results for 100-Cr are presented in Figure 4.15. The data shows a strong relationship between temperature and ductility as the 280°C sample exhibits a large plastic deformation. Both the 230°C and 180°C samples showed only a limited amount of plastic straining. This suggests there is a pronounced dependence of the mechanical properties on temperature. Samples follow traditional ductile to brittle behavior with the highest temperature samples achieving the largest percent reduction in area (Table 4.11). Also there is a sharp transition between 230°C and 280°C.

Table 4.11: Summary of Results for 100-Cr Elevated Temperature Tensile Test

Sample Number	% RA	σ_{uts} (MPa)	σ_y (MPa)
R7-T6-1-280C	60.9	281.8	227.4
R7-T6-2-230C	3.6	287.5	231.8
R7-T6-3-180C	2.2	275.4	216.3

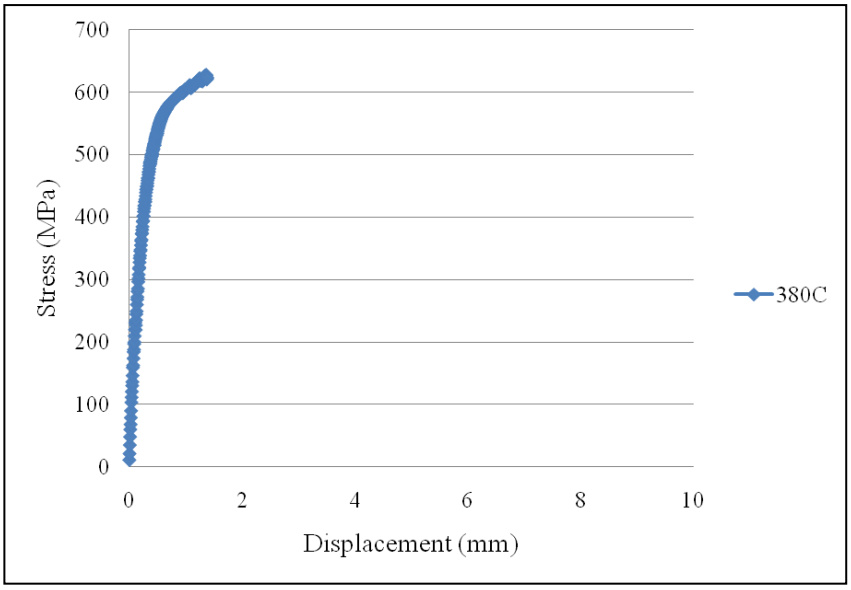

Figure 4.16: Elevated Temperature Tensile Results for 75Cr-25V

From Figure 4.16 and Table 4.12 it can be seen that the 75Cr-25V had a small reduction in area at 380°C and the sample exhibits mostly brittle behavior. Only one sample was tested as the results from this test confirmed the bend data at 380°C.

Table 4.12: Summary of Results for 75Cr-25V Elevated Temperature Tensile Test

Sample Number	% RA	σ_{uts} (MPa)	σ_y (MPa)
R8-T6-1-380C	1.7	627.6	432.2

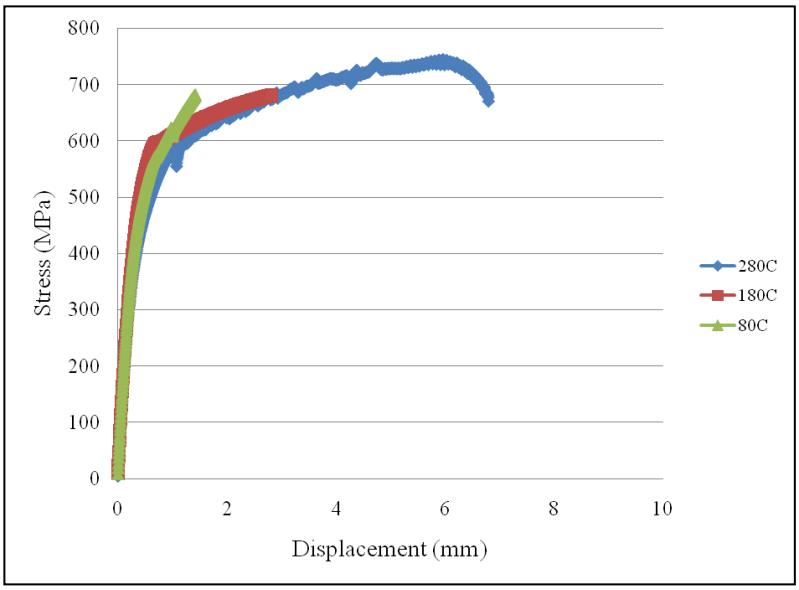

Figure 4.17: Elevated Temperature Tensile Results 25Cr-75V

From Figure 4.17 it can be seen there is a strong relationship between testing temperature and tensile behavior for the 25Cr-75V alloy. With a large plastic regime and a reduction in area of 30.2%, the 280°C specimen exhibits ductile behavior. At 180°C less strain is observed but a plastic regime is still observed as the specimen shows some ductility. Finally at 80°C the specimen shows no ductility and no measurable amount of reduction in area occurs.

Table 4.13: Summary of Results for 25Cr-75V Elevated Temperature Tensile Test

Sample Number	%RA	σ_{uts} (MPa)	σ_y (MPa)
R10-T6-1-280C	30.2	744.12	406.4
R10-T6-2-180C	5.7	681.2	476.6
R10-T6-3-80C	0	681.9	445.5

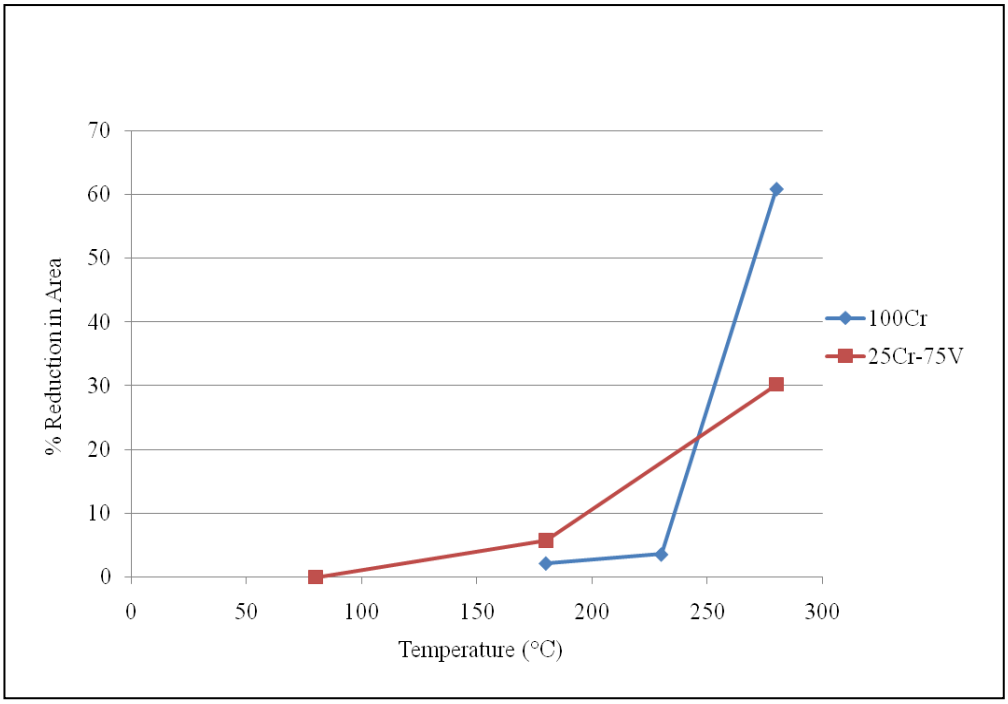

Figure 4.18: Reduction in Area as a Function of Temperature for Elevated Temperature Tensile Specimens

For the specimens which exhibit a temperature dependence on tensile ductility a plot of reduction in area versus temperature is shown in Figure 4.18. For the 100-Cr sample a sharp change in the reduction in area transitions from 3.6% to 60.9% between 230°C and 280°C. For the 25Cr-75V the change in reduction in area is a more gradual transition from 5.7% to 30.2% from 180°C to 280°C.

4.3 Fracture Surface Analysis

4.3.1 100 Cr 3-Point Bend Fracture Surfaces

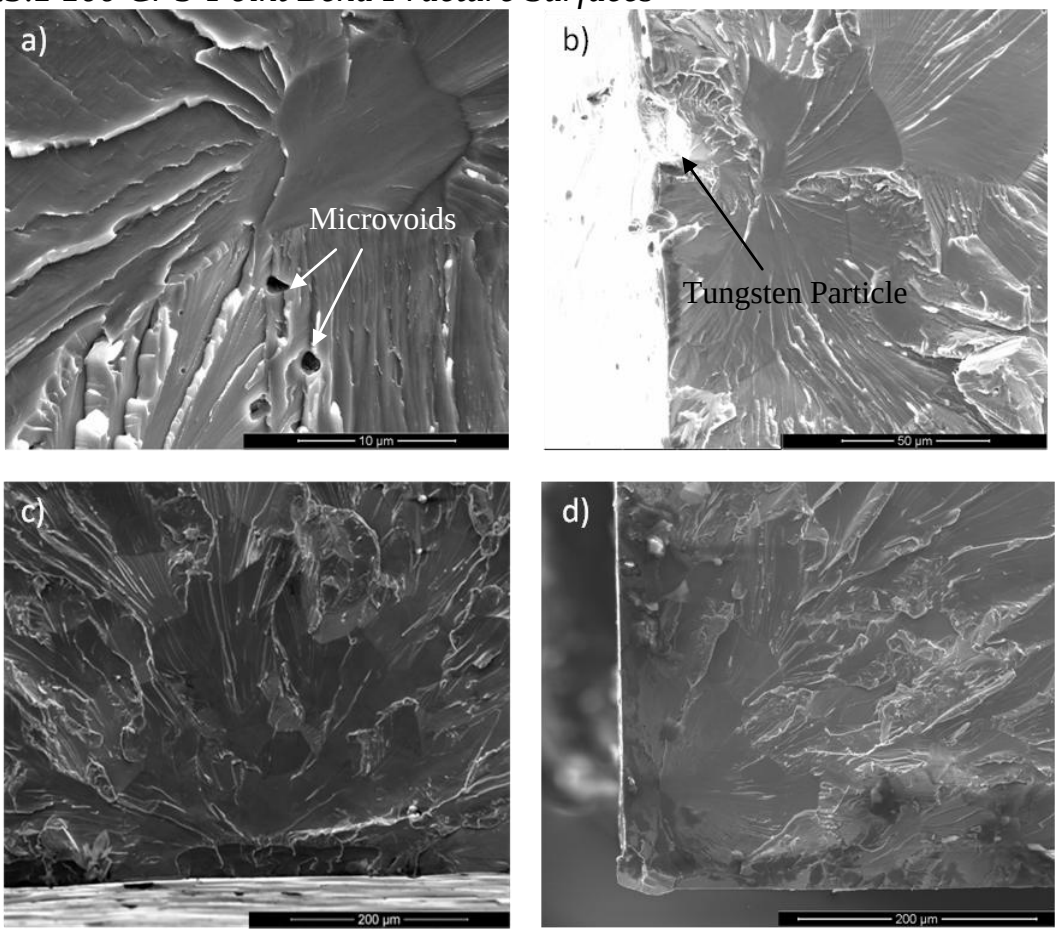

Figure 4.19: Fracture Surface of 100-Cr Showing Origin of Fracture in Elevated Temperature *3-point* Bend Specimens a)180°C (Electropolish) b)80°C (Electropolish) c)80°C (Mechanical Polish) d)21°C (Mechanical Polish)

Following the river markings in the 100-Cr bend samples, the sources of failure were located. Due to higher stress concentrations failure frequently initiated at an edge or corner as can be seen in Figure 4.19 b-d. In the 180°C sample the source of failure was found to be very near a region of microvoids, near the center of the sample. A tungsten rich particle was found at the center of the source of failure in the 80°C electropolished specimen. All samples failed by transgranular cleavage which is characteristic of chromium likely on the {110} planes.

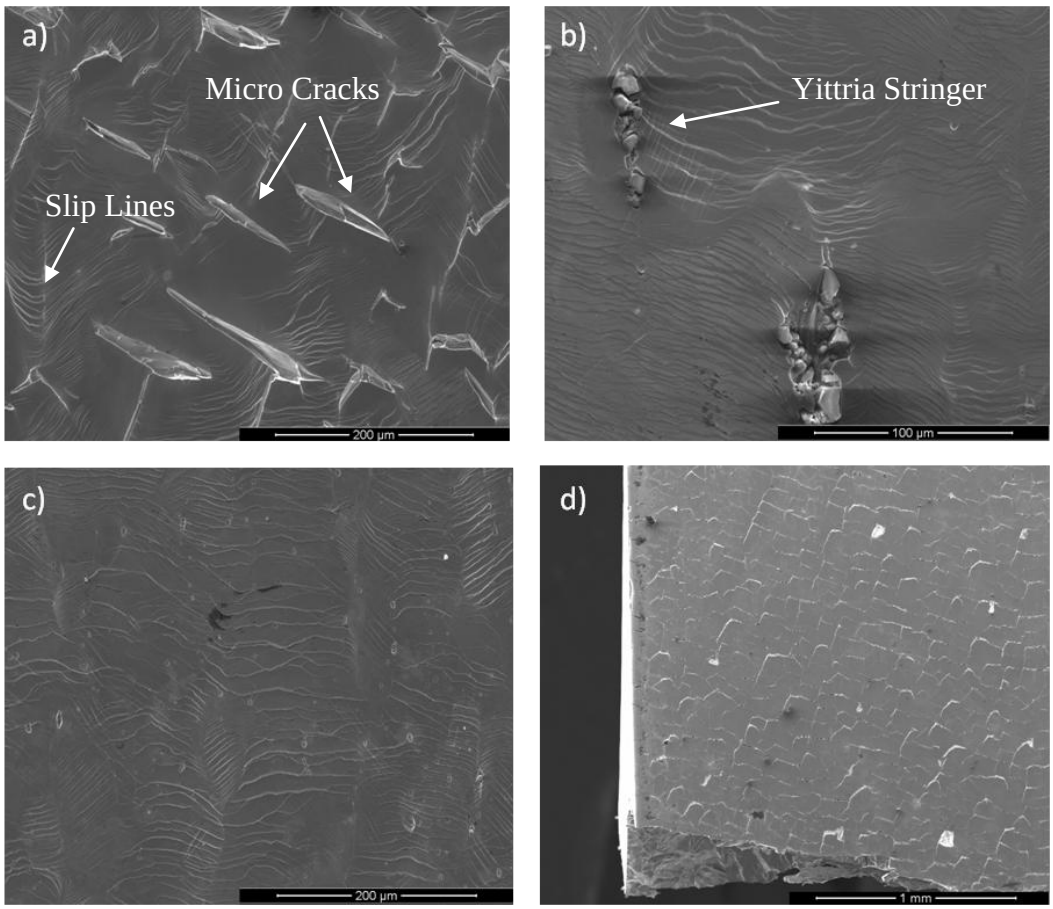

Figure 4.20: Tensile Surface of 100Cr Elevated Temperature *3-point* Bend Specimens a) 280°C b) 230°C c)380°C d)80°C (Mechanical Polish)

The tensile, surface of 100-Cr bend samples can be found in Figure 4.20. A combination of microcracking and slip lines, indicative of a transition in failure mechanisms, can be observed in the 280°C sample. At 380°C and 230°C only slip lines are found on the sample, signaling ductile failure. In Figure 4.20b yittria stringers are also found on the tensile surface. Finally, at 80°C extensive microcracking is found on the surface of the materials indicating brittle failure (Figure 4.20d).

4.3.2 75Cr-25V 3-Point Bend Fracture Surfaces

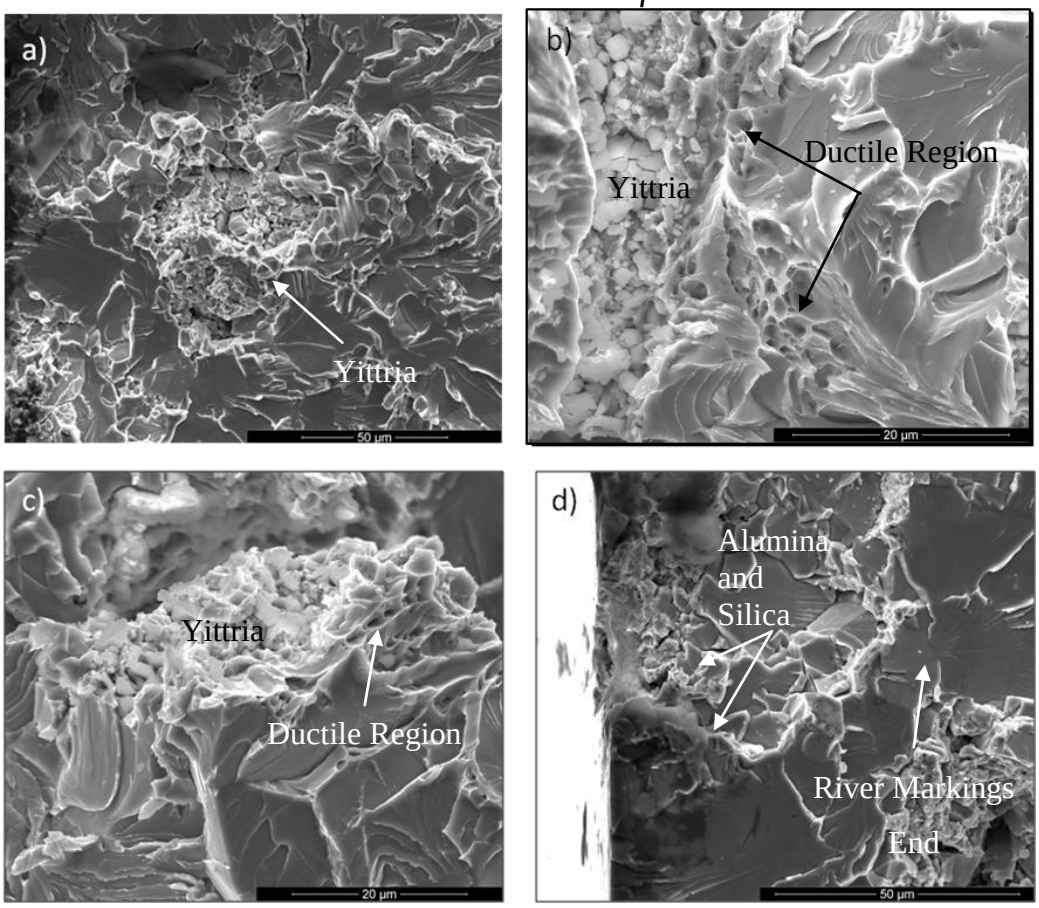

Figure 4.21: Fracture Surface of 75Cr-25V Elevated Temperature *3-point* Bend Specimens a)380°C-2 b) 330°C-2 c) 330°C-1 d) 380°C-1

The fracture surfaces of 75Cr-25V are found in Figure 4.21. At 380°C a large particle of yittria found near the corner of the sample is (Fig 4.21a) believed to be the source of failure. Figure 4.21b shows a localized region of microvoid coalescence indicative of ductile failure. Figure 4.21c shows another small region of ductile fracture where microvoid coalescence can be seen, as marked by a white arrow. Following the river markings in 380°C sample #1 a suppressed region, likely a crack, was located and is the source of failure in this sample (Figure 4.21d). Additionally in the crack on the tensile edge of the specimen silica and alumina polishing compound were located providing more evidence this was a pre-existing crack.

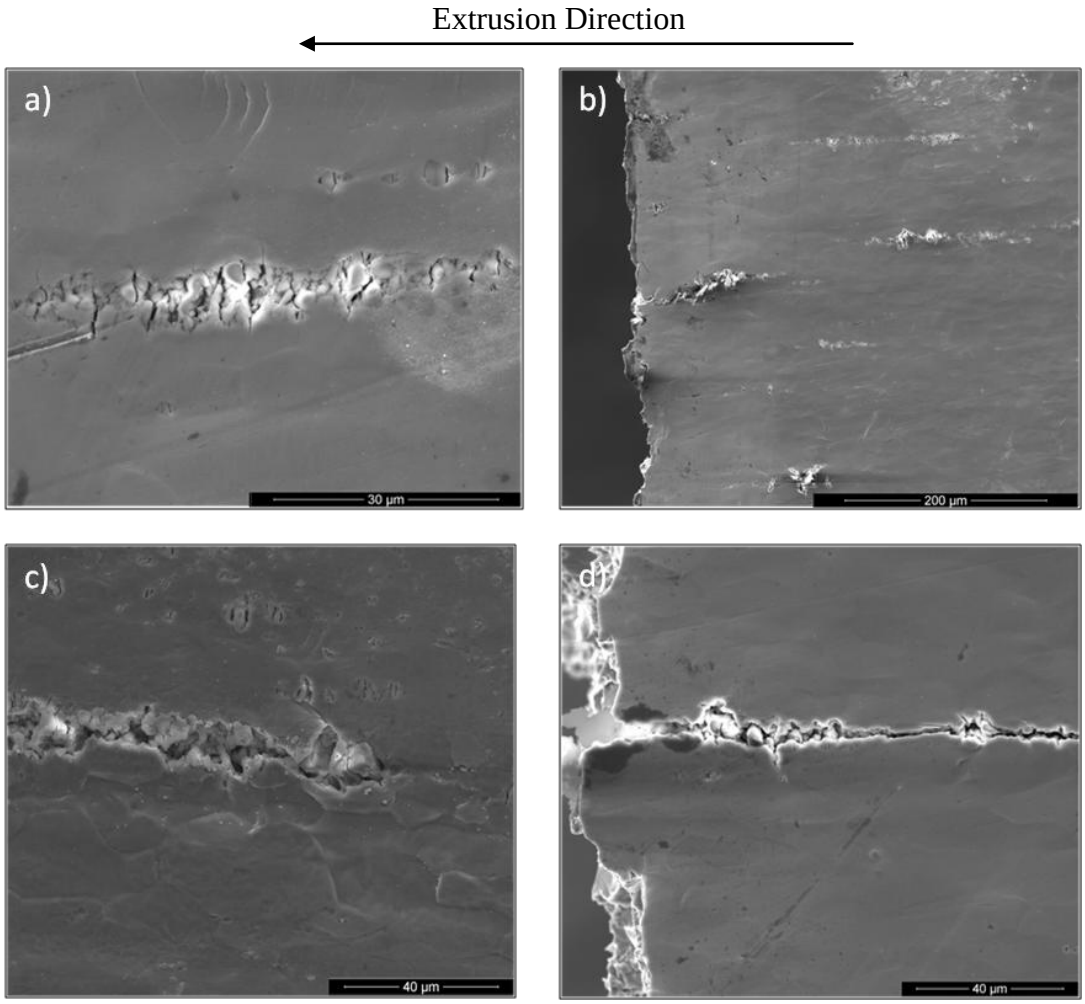

Figure 4.22: Tensile Surface of 75Cr-25V Showing Yittra Stringers on Tensile Surface of 3-point Bend Specimens a) 380°C-2 b) 380°C-1 c) 330°C-1 d)330°C-1

Yittra 'stringers' were found on the tensile surface of all 75Cr-25V samples at a frequency of ~20-30 stringers/mm^2 and an approximate length of 100 micrometers (Figure 4.22). Stringers were likely produced during extrusion as silica and alumina polishing compound can be found in them. Typically orientated in the tensile stress direction these stringers do not appear to grow into cracks during flexural loading as the edges are typically round and blunted. In Figure 4.22a the sample shows a small amount of slip lines suggesting some ductility.

4.3.3 50Cr-50V 3-Point Bend Fracture Surfaces

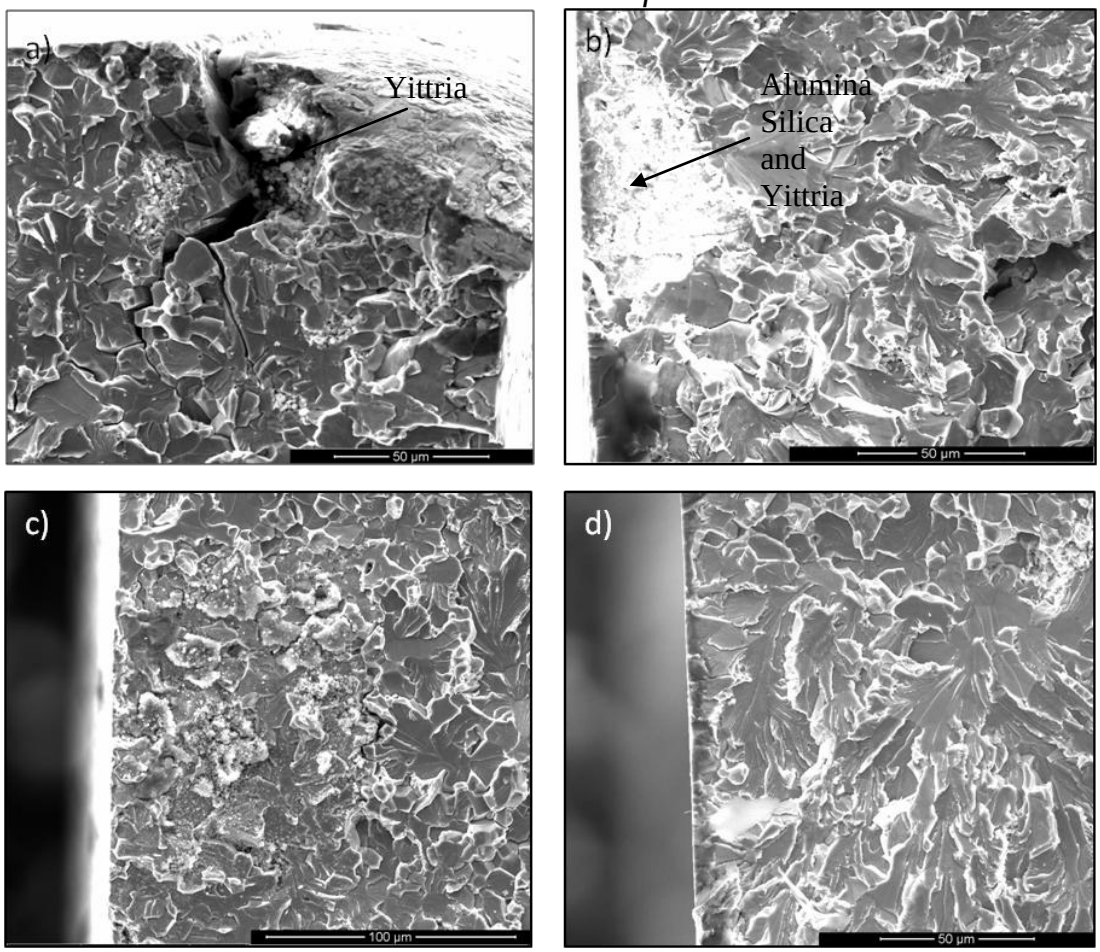

Figure 4.23: Fracture Surface of 50Cr-50V Elevated Temperature *3-point* Bend Specimens a) 280°C b) 380°C c) 330°C d) 180°C

The fracture surface of the 280°C 50Cr-50V sample shows a large crack at the edge, likely the source of fracture, with a large yittra particle in the center (Figure 4.23a). The 380°C sample also shows damage at the edge of the sample with large amounts of yittria as well as silica and alumina (Figure 4.23b). However, for both the 330°C and 180°C samples no obvious failure sources were found at the edges and they demonstrated pure transgranular cleavage fracture (Figures 4.23c and 4.23d).

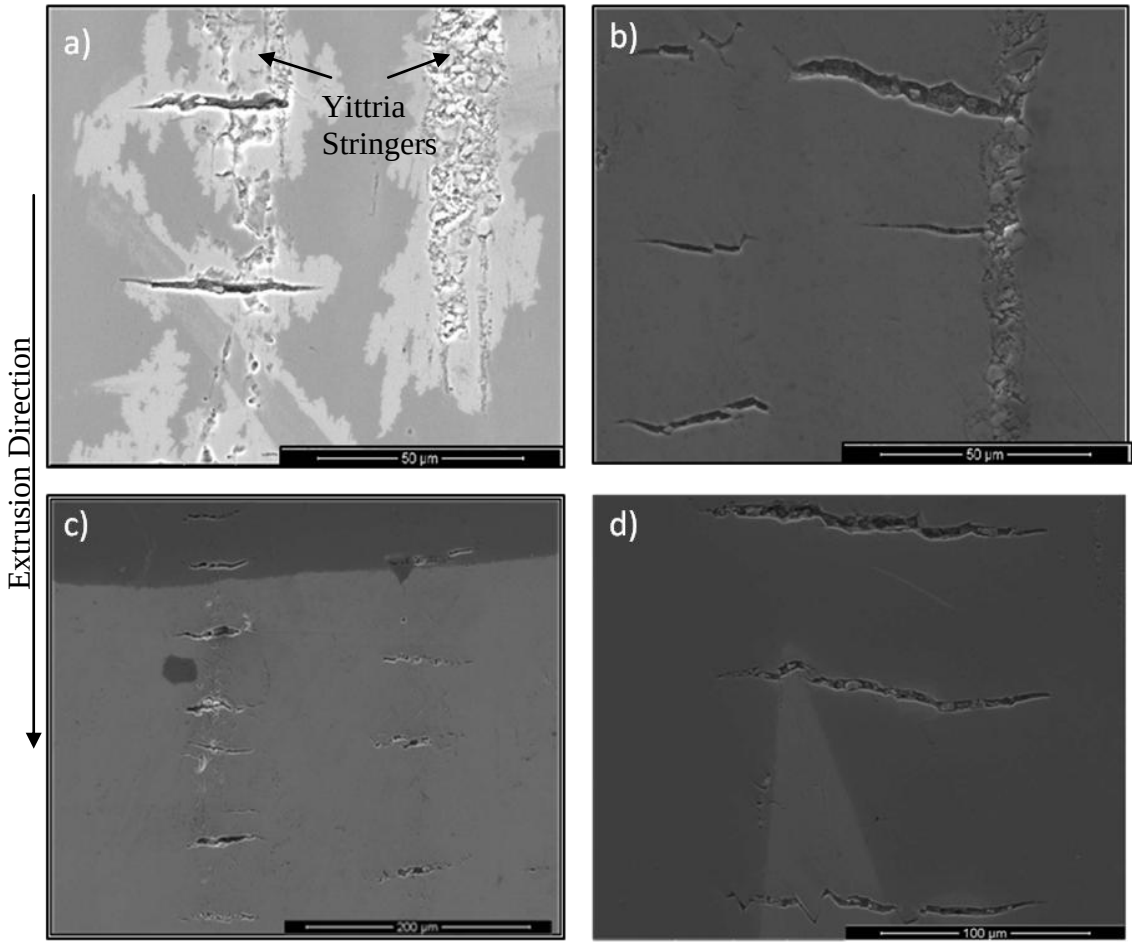

Figure 4.24: Tensile Surface of 50Cr-50V *3-point* Bend Specimens
a)280°C b)380°C c)180°C d)380°C

On the tensile surface of all 50Cr-50V samples evidence of pre-existing, mechanical damage and cracking was found (Figure 4.24). Cracking was believed to be pre-existing as alumina and silica polishing compound could be found in them by EDS. Some of the largest cracks were found to be >150µm. Always found in columns, the cracks were oriented perpendicular to the applied force during testing allowing brittle fracture to occur well below the yield strength.

4.3.4 25Cr-75V 3-Point Bend Fracture Surfaces

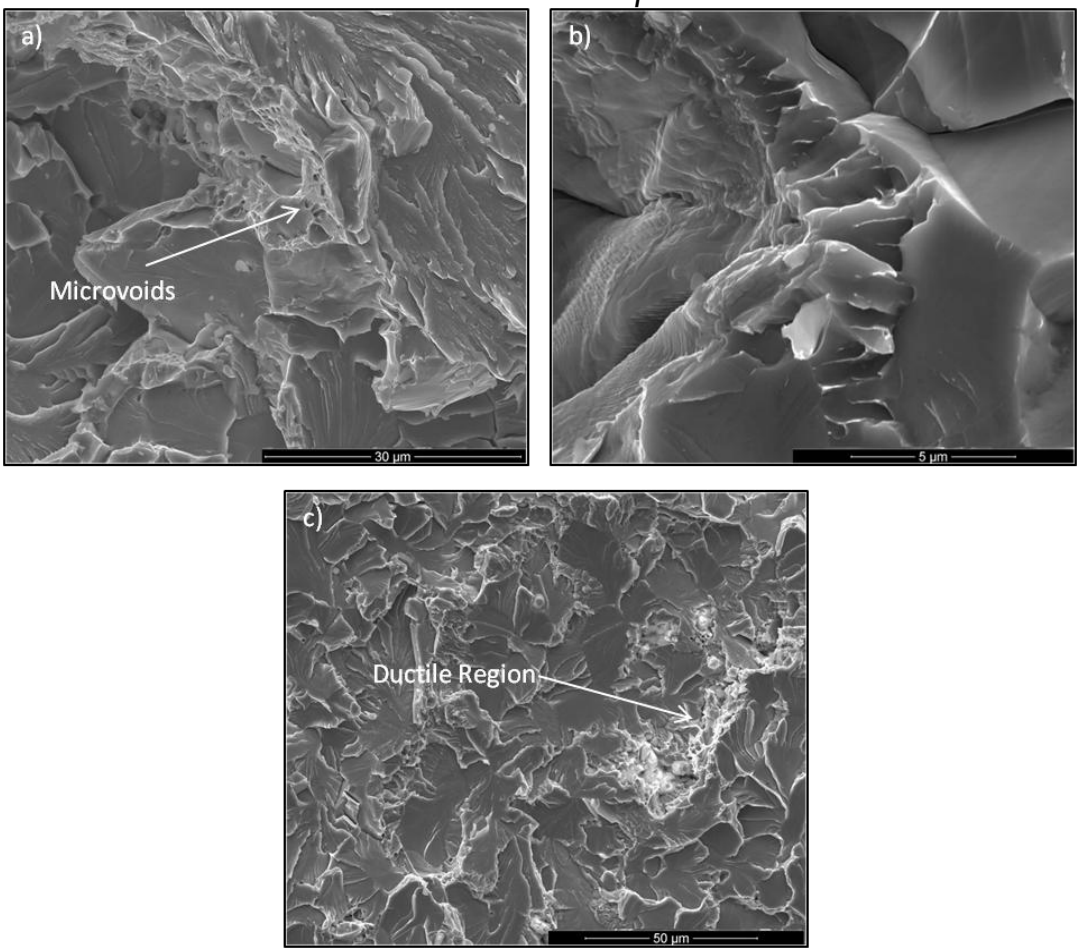

Figure 4.25: Fracture Surface of 25Cr-75V *3-point* Bend Specimens
a)280°C b)380°C c)180°C

Some microscale ductility was observed in the 25Cr-75V samples as can be seen from Figure 4.25a and 4.25b. A small region (~10µm) of microvoids can be seen along the edge of a grain boundary in the 380°C sample (Figure 4.25b). In the 280°C sample a region of less than 20 micrometers in length of concentrated microvoids can be seen, indicating some ductility (Figure 4.25a). At 180°C small regions of microvoid coalescence were located within the largely cleavage fracture planes (Figure 4.25c).

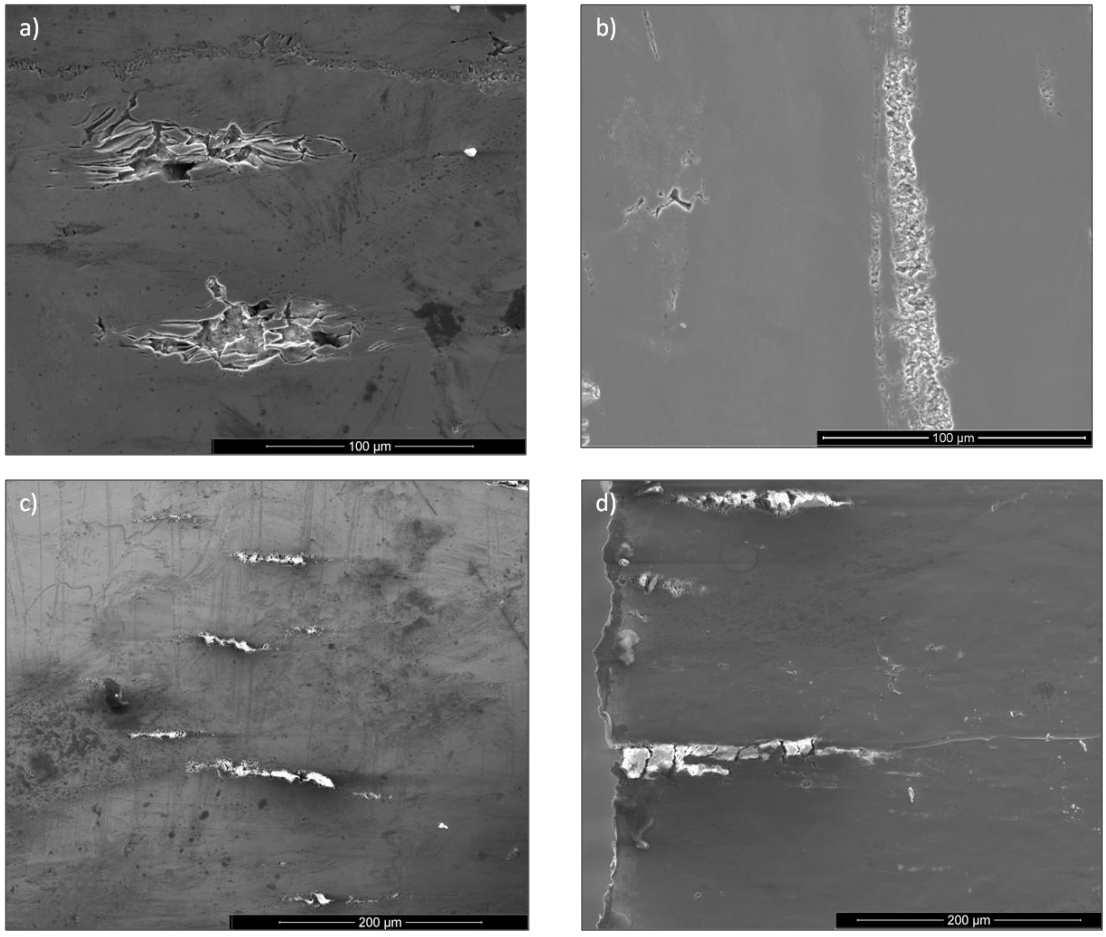

Figure 4.26: Tensile surface of 25Cr-75V showing tensile surfaces of *3-point* bend specimens a) 180°C b) 330°C c) 230°C d)230°C

Pre-exisiting damage found on the tensile surface of 25Cr-75V bend specimens was determined to be a combination of both yittra stringers and extrusion damage (Figure 4.26). In all cases the damage was determined to occur prior to testing as edges of the cracks were blunted and did not appear to grow during testing. Additionally, polishing compound in the cracks was identified.

4.3.5 100Cr Elevated Temperature Tensile Fracture Surfaces

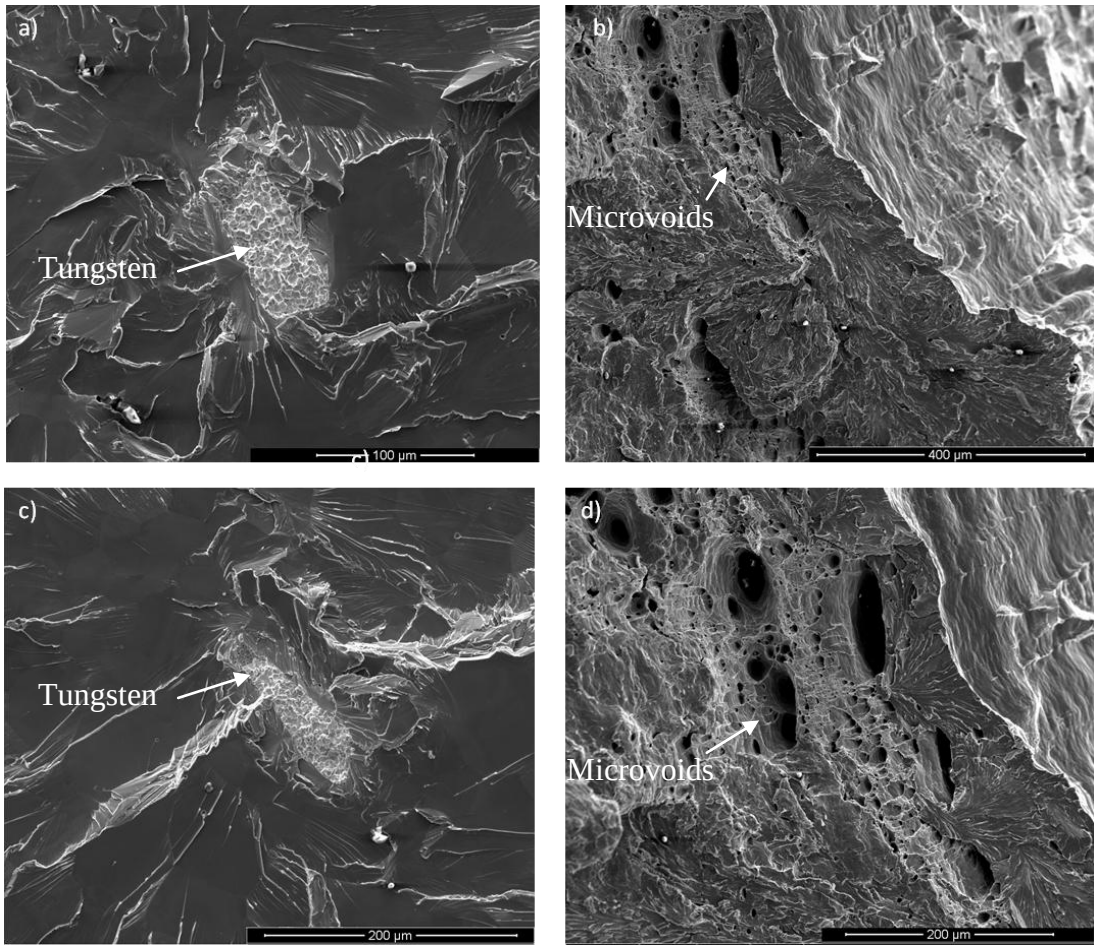

Figure 4.27: Fracture Surface of 100-Cr Elevated Temperature Tensile Specimens a)230°C b)280°C c)180°C d)280°C

The elevated temperature tensile specimens of pure chromium exhibited both ductile and brittle behavior as can be seen from the fracture surfaces in Figure 4.27. In both the 230°C and 180°C specimens the source of failure was located and a large (>100µm) tungsten rich particle was found at the center. The 280°C sample shows a very ductile fracture surface as large areas of microvoids were found (~100µm).

4.3.6 25Cr-75V Elevated Temperature Tensile Fracture Surfaces

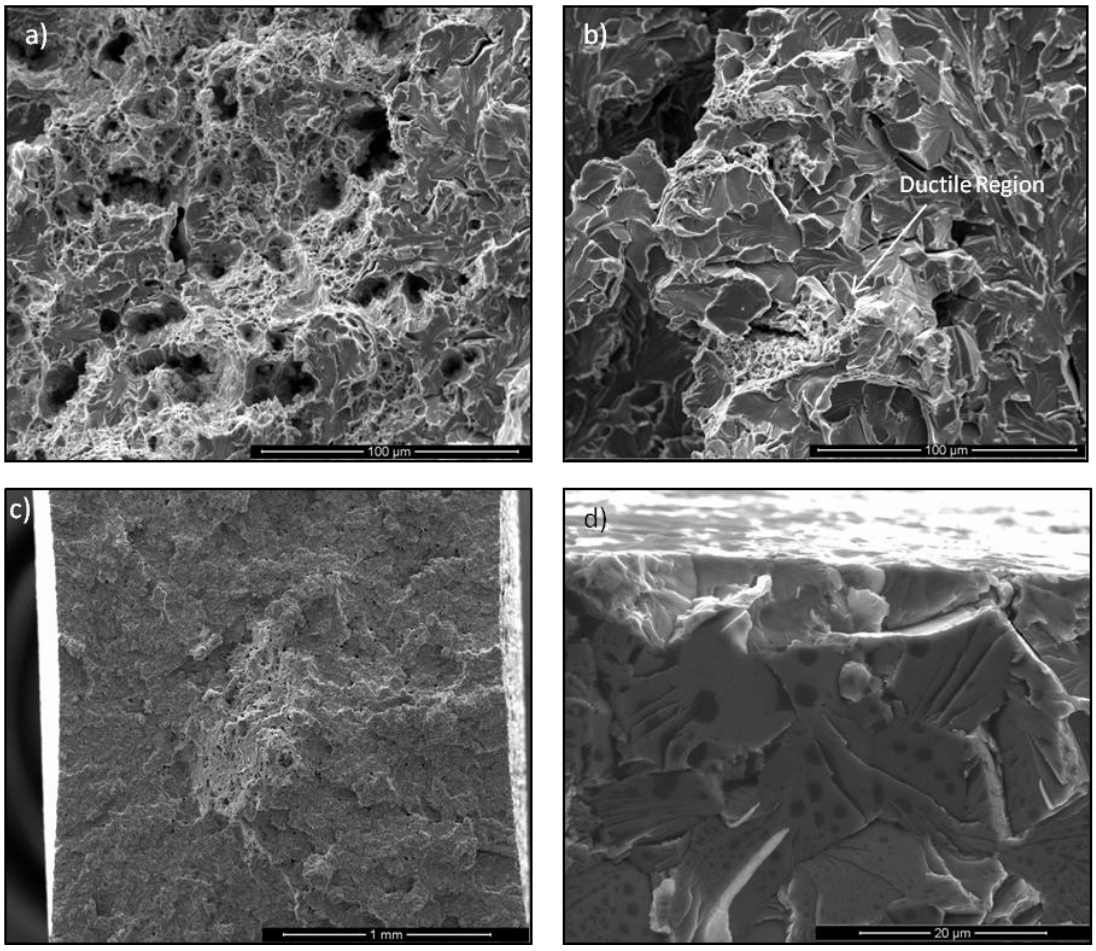

Figure 4.28: Fracture Surface of 25Cr-75V Elevated Temperature Tensile Specimens a)280°C b)180°C c)280°C d)80°C

The fracture surfaces of the 25Cr-75V samples shows a strong dependence of fracture type on temperature. At 280°C the sample shows large scale ductility as cup and cone fracture with large voids found on the entire fracture surface (Figures 4.28a and 4.28c). From Figure 4.28b regions of microvoid coalescence are observed inside the transgranular cleavage fracture regions showing both the ductile and brittle behavior of the specimen at 180°C. At 80°C the specimen fails entirely by brittle cleavage fracture incited by a small microcrack at the edge of the sample (Figure 4.28d).

4.3.7 75Cr-25V Elevated Temperature Tensile Fracture Surfaces

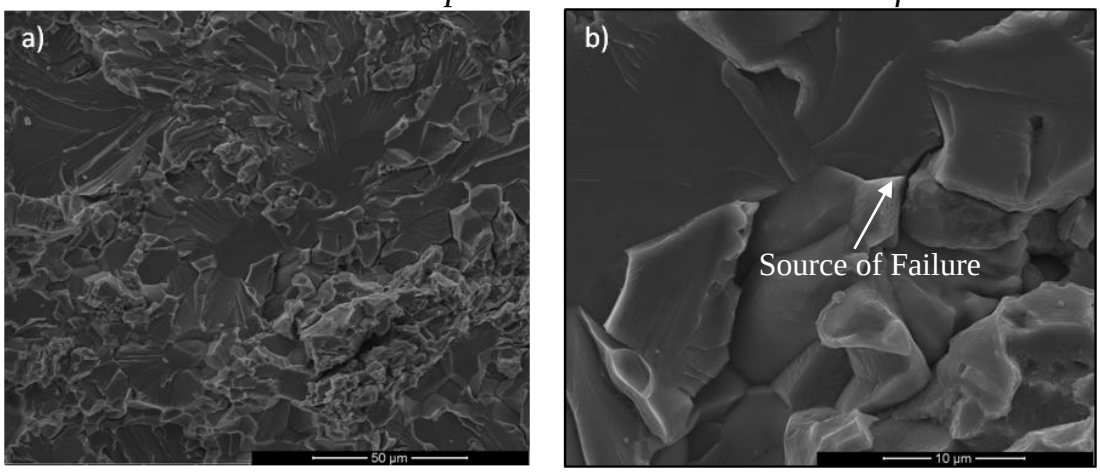

Figure 4.29: Fracture Surface of 75Cr-25V Elevated Temperature Tensile Specimen at 380°C

The fracture surface of 75Cr-25V shows brittle cleavage fracture as the primary mode of failure at 380°C (Figure 4.29).

4.4 Fracture Toughness Calculations

Results and values used in the fracture toughness calculation are summarized in Table. 4.14, Figure 4.30 shows the surface crack which was used for the calculation, the crack measured to be 165.2 micrometers in length, it was assumed to have a crack depth of 82.6 micrometers.

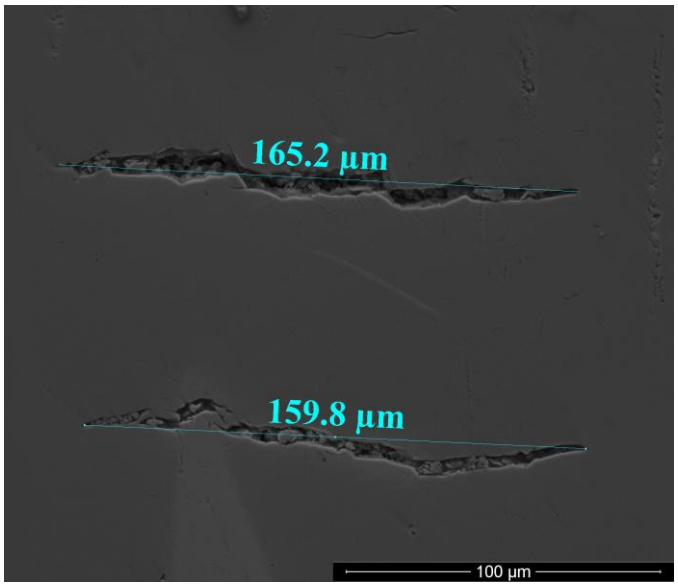

Figure 4.30 Largest Surface Crack Found in the Unstressed Region of a 50Cr-50V Elevated Temperature *3-point* Specimen

Table 4.14: Summary of Values Used for Fracture Toughness Calculations

Variable	Value	Variable	Value	Variable	Value
a	8.26E-05	g	1.10	H_1	0.99
c	8.26E-05	fφ	1	H_2	0.96
Q	2.464	f_w	1.00	p	1.22
M_1	1.04	Fs	1.14	Hs	0.99
M_2	2.02E-01	G_{21}	-1.34		
M_3	-1.06E-01	G_{22}	-0.03		

K_I (MPa√m)	7.8

The fracture toughness value for this specimen was calculated to be 7.8 MPa√m which for a metal is considered to be quite brittle.

5.0 Discussion

5.1 Processing

Achieving a homogeneous mixture beginning with 50 micron powders took much consideration and was not fully achieved. Using electron microprobe data a diffusivity was calculated and it was determined that developing a homogenizing heat treatment was unrealistic with a diffusion alone. A diffusivity for Cr-V of roughly $2.2 \times 10^{-11} \frac{cm^2}{s}$ at 1300°C compared to the published diffusivity of $2.4 \times 10^{-12} \frac{cm^2}{s}$ at 1200°C shows a disparity. [48] The difference between the two values could be due to the 1-D assumption that was used in these calculations. However, in an effort to increase the homogenization of the samples by reducing the diffusion distance extrusion was used as a way of increasing the homogeneity of the samples.

Extrusion was performed to both increase the strength by decreasing the grain size but also to further mixing of the material and reduce the diffusion distance. As can be seen from the microprobe and x-ray diffraction data the extruded samples were more homogeneous than the heat treated samples. The extrusion initially appeared to have a positive effect on the strength of the samples as an increase in the hardness was observed relative to the heat treated samples. This effect was likely due to a decrease in average grain size and strengthening via substitutional alloying.

5.2 Mechanical Testing

Data from the hot hardness testing suggest a factor of two increases in the strength of chromium when alloyed with vanadium. There is good agreement between the elevated temperature Vickers hardness and elevated temperature *3-point* bend test; for example the yield strength of 100Cr in hardness and bend is 361MPa and 375MPa respectively. However, tensile test revealed a much lower yield strength, which may suggest an asymmetry in the tensile and compressive yielding behavior.

5.2.1 Pure Chromium Samples

It has been noted that chromium is extremely notch sensitive and microcracks in the surface of samples is sufficient for premature failure.[15] However, results from the 3-point bend tests indicate that chromium is not sensitive to the surface conditions between this mechanical polishing technique and electropolishing, as samples tested at similar temperatures displayed similar failure strain values. Comparing the results from the 100-Cr electropolished and mechanical polished bend test, it is noted that the bend transition temperature is likely to be between 180°C and 230°C, corresponding to a tensile transition temperature between 230°C and 280°C for pure chromium in the extruded condition.

As previously reported high impurity contents will embrittle pure chromium at room temperature. The DBTT range achieved (230°C-280°C) is higher than reported by Braint et.al.(175°C) with forged chromium samples of similar nitrogen impurities (~50ppm) but higher C levels (~ 200ppm). [26] It was later found that samples which contained >50ppm C exhibited no ductility and failed by transgranular cleavage which agrees with the noted mode of failure in these samples.[25] Futher, yittria which was added as a getter to remove N and O was determined by Ryan et al. to not getter C.[22]

Carbon may have contributed to the microscale embrittlement of chromium but tungsten rich particles are the source of failure in the pure chromium samples. This result is similar to Kurshita who found large tungsten particles in PM samples after ball milling powders before compaction.[40] It is believed that powder preparation prior to compaction is the source of tungsten rich particles and premature failure of the pure chromium samples.

5.2.2 Chromium Vanadium Samples

For the chromium samples containing vanadium, extrusion appears to have caused cracking and yittria stringers observed in the surface of all bend samples. Compared with Kurshita et al. with similar yittria content, they did not observe these stringers in cold rolled samples.[40] The negative effects of extrusion also seems to

be a function of % homogeneity of the initial samples, as the samples with the most extrusion induced damage appear to be the least homogeneous initially, i.e., 50Cr-50V.

5.2.3 75Cr-25V Samples

Embrittlement from pre-existing mechanical damage in 75Cr-25V caused premature failure; as evident by the scattered *3-point* bend results and SEM analysis where polishing compounds were found in the cracks. Additionally these samples did not follow a typical DBTT behavior as was expected suggesting surface damage was causing failure rather than intrinsic properties. However, regions of microvoid coalescence found in the 330°C samples suggest ductility could have been achieved.

5.2.4 50Cr-50V and 25Cr-75V Samples

Extrusion is likely the source of cracking observed in the 50Cr-50V samples. Due to the extreme variability in the bend data these cracks are believed to be the cause of pre-mature failure as some of the largest cracks in the unstressed region were >150μm. Due to the large cracks found in the bend specimens, tensile specimens were not tested. Fracture toughness calculations further confirmed the brittleness in the 50Cr-50V as a K_1 was found to be quite low, 7.8 MPa$\sqrt{m}$. Conversly the reported results from Kurshita et. al. found 52Cr-1.8Y-V mechanically alloyed powder metallurgy samples were ductile in room-temperature tensile tests, exhibiting a total reduction in area of 22-32% and a total elongation of 10-19%.[40]

Fracture surface analysis was used to determine the bend transition temperature of 25Cr-75V samples as quantitative ductility results were inconclusive. The fracture surfaces suggest the transition temperature is below 180°C as regions of microvoid coalescence are observed on the fracture surface of all specimens. The reduction in area curve for 25Cr-75V suggests a gradual transition between ductile and brittle behavior around 180°C. This is supported by the fracture surface results which show large scale ductile fracture (~1mm^2) among the cleavage fracture planes at 180°C. The ductile region is believed to contain the source of failure and therefore, the tensile transition temperature is believed to be between 180°C and

80°C for which a total reduction in area of 5.7% at 180°C and 0% at 80°C was observed. This result is clearly different from Kurshita et. al. which found 28Cr-2.3Y-V to be ductile at room temperature, achieving a total reduction in area of >55%.[40] The room temperature ductility in those samples is accredited to the advanced mechanical alloying and HIPing techniques that were used to achieve a homogenous mixture.[40]

Inhomogenities of these samples is likely the source of premature failure and cracking during extrusion as vanadium and chromium presumably deform at different rates resulting in localized tensile stresses. The differences in the localized strain rates are believed to have caused much of the pre-existing mechanical damage observed in the specimens. The advanced techniques, mechanical alloying and powder metallurgy, employed by Kurshita et. al. eliminated the need for additional processing or extruding. The processing techniques used by Kurshita et. al. are believed to be the source of superior mechanical properties in similar compositions.

Finally, the 100Cr samples exhibited either extreme ductility and did not fracture or transgranular cleavage fracture with no ductile regions. As reported by Kurshita vanadium has impact on the overall ductility of the chromium, and it is likely vanadium contributed to the ductility of the Cr-V samples.[40] Mechanical damage and inhomogeneities caused the premature brittle fracture of the Cr-V samples as Kurshita et. al. successfully prepared ductile room temperature tensile specimens of similar compositions.[40] Further testing of the Cr-V samples is needed to confirm vanadium's impact on the ductility of chromium using a processing technique that will not cause mechanical damage.

6.0 Conclusions

Cr-V samples were prepared using powder metallurgy processes, heat treated at 1300°C, then extruded at a 6:1 ratio. Materials were subjected to a series of electron microprobe and x-ray diffraction analysis to determine homogeneity with processing. Vickers hot hardness, *3-point* bend and elevated temperature tensile testing was performed to measure the effects of processing and vanadium on the ductility of chromium. The most significant results are as follows:

- The calculated diffusivity of chromium into vanadium determined heat treating at 1300°C to be insufficient to attain a homogenous material.
- Extrusion of samples provided a more compositionally homogeneous test material, but induced damage in the Cr-V alloys where the initial alloys were highly inhomogeneous. The most extrusion induced damage occurred in the least homogeneous samples, i.e., 50Cr-50V.
- Hot hardness data revealed vanadium to have increased the hardness by a factor of two. Extrusion also increased the hardness of all alloys, likely due to the refined grain size.
- Fracture surface analysis revealed damage induced during extrusion was the cause of pre-mature failure in the 75Cr-25V, 50Cr-50V and 25Cr-75V bend samples, however, regions of microvoid coalescence in the 25Cr-75V and 75Cr-25V samples suggest that vanadium has a ductilizing effect on chromium and further testing must be done on undamaged samples to fully evaluate this effect.
- Combining the tensile data and the bend data with fractography the ductile-to-brittle transition temperature of pure chromium in the extruded condition is believed to be between 230°C and 280°C in tension and between 180°C and 230°C in bending.

- Fracture surface analysis and elevated temperature tensile results for the 25Cr-75V samples in the extruded form showed vanadium had an impact on the ductility of chromium as the transition temperature is believed to be between 180°C and 80°C. This is lower than for pure chromium and again indicative of the ductilizing effect.

For any refractory material to be commercially exploited, superior mechanical properties must be achieved, integrated into a workable design and with an affordable method of fabrication. Inhomogeneties in Cr-V samples cause localized strains which resulted in cracking and mechanical damage of extruded samples. For the Cr-V system to be successful, processing techniques must be developed which will achieve sufficient homogeneity and mechanical properties. Further testing of Cr-V materials without the use of extrusion as a means of increasing homogeneity is proposed.

References

[1] Dimiduk DM, Perepezko JH. Mo-Si-B alloys: Developing a revolutionary turbine-engine material. Mrs Bulletin 2003;28:639.
[2] Perepezko JH. The Hotter the Engine, the Better. Science 2009;326:1068.
[3] Bewlay BP, Jackson MR, Zhao JC, Subramanian PR. A review of very-high-temperature Nb-silicide-based composites. Metallurgical and Materials Transactions a-Physical Metallurgy and Materials Science 2003;34A:2043.
[4] Briant CL. The use of refractory metals as high temperature structural materials. Journal of Engineering and Materials Technology 2000;122:338.
[5] Jehanno P, Boning M, Kestler H, Heilmaier M, Saage H, Kruger M. Molybdenum alloys for high temperature applications in air. vol. 51: Maney Publishing, 2008:99.
[6] Bewlay BP, Jackson MR, Subramanian PR. Processing high-temperature refractory-metal silicide in-situ composites. Jom-Journal of the Minerals Metals & Materials Society 1999;51:32.
[7] Mitra R. Mechanical behaviour and oxidation resistance of structural silicides. International Materials Reviews 2006;51:13.
[8] Heilmaier M, Kruger M, Saage H, Rosler J, Mukherji D, Glatzel U, Volkl R, Huttner R, Eggeler G, Somsen C, Depka T, Christ HJ, Gorr B, Burk S. Metallic materials for structural applications beyond nickel-based superalloys. Jom 2009;61:61.
[9] Burk S, Gorr B, Trindade VB, Krupp U, Christ HJ. High temperature oxidation of mechanically alloyed Mo-Si-B alloys. Corrosion Engineering Science and Technology 2009;44:168.
[10] Kruzic J. Development of High Temperature Refractory Metal Based Alloys. 2007.
[11] Carter TJ. Common failures in gas turbine blades. Engineering Failure Analysis 2005;12:237.
[12] Oryshich IV, Poryadchenko NE, Slys IG, Brodnikovskii NP, Golovash AV. Air oxidation of chromium-based composites. Powder Metallurgy and Metal Ceramics 2007;46:189.
[13] Sims CT. The Case for Chromium. Journal of Metals 1963;15:5.
[14] Portini KI, Babich BI. Dispersion Hardened Materials. Moscow, 1974.
[15] Gu YF, Harada H, Ro Y. Chromium and chromium-based alloys: Problems and possibilities for high-temperature service. Jom 2004;56:28.
[16] Hook R, Adair A. On the Recrystallization Embrittlement of Chromium. Transactions of the Metallurgical Society of AIME 1963;227:151.
[17] Gilbert A, Reid CN, Hahn GT. Observations on the Fracture of Chromium. Journal of the Institute of Metals 1964;92:351.
[18] Hook RE, Adair AM, Lipsitt HA. Observations on the Ductlity and Fracture of Recrystallized Chromium. Transactions of the Metallurgical Society of AIME 1961;221:409.

[19] Solie KE, Carlson ON. The Effect of Nitrogen on the Brittle-Ductile Transition of Chromium. Transations of the Metallurgical Society of AIME 1964;230:480.
[20] Sully AH, Brandes EA, Mitchell KW. The Effect of Temperature and Purity on the Ductility and Other Properties of Chromium. Journal of The Institute of Metals 1952-1953;81:585.
[21] Gu YF, Ro Y, Harada H. The Possibility of Cr-base Alloys for High-Temperature Applications. Materials Science Forum 2005;475-479:627.
[22] Ryan NE. An Appraisal of Possible Scavenger Elements for Chromium and Chromium Alloys. Journal of the Less-Common Metals 1964;6:21.
[23] Smith WH, Seybolt AU. The Effect of Impurity on the Ductility of Chromium. ASM. Materials Park, Ohio, 1957:169.
[24] Isshiki M, Arakawa K, Igaki K, Mizohata A, Tsujimoto T. Prepartion of High-Purity Chromium. Journal of the Less-Common Metals 1984;96:157.
[25] Briant CL. Impurity effects in chromium and titanium. Materials Transactions Jim 2000;41:161.
[26] Briant CL, Kumar KS, Rosenberg N, Tomioka H. The mechanical properties of high purity chromium. International Journal of Refractory Metals & Hard Materials 2000;18:9.
[27] Henderson F, Johnston STM, Wain HL. The Effect of Nitride-Formers upon the Ductile-To-Brittle Transition in Chromium. Journal of the Institute of Metals 1964;92:111.
[28] Abrahamson II EP, Grant NJ. Brittle to Ductile Transition Temperatures of Binary Chromium-Base Alloys. Transactions of the ASM 1957;50:705.
[29] Wain HL, Henderson F, Johnstone STM, Louat N. Further Observations on the Ductility of Chromium. Journal of The Institute of Metals 1957-1958;86:281.
[30] Wadsack R, Pippan R, Schedler B. The effect of pre-deformation on the ductility of chromium. 2000:701.
[31] Matsumoto Y, Ohta S, Aoki N, Morinaga M. Microscopic fracture mechanism of sintered high purity chromium. Materials Science and Engineering a-Structural Materials Properties Microstructure and Processing 2000;285:213.
[32] Bourcier RJ, Koss DA, Smelser RE, Richmond O. The Influence of Porosity on the Deformation and Fracture of Alloys. Acta Metallurgica 1986;34:2443.
[33] Carlson ON, Sherwood LL, Schmidt FA. The Effect of Low Percentage Alloying Addtion on the Ductility of Iodide Chromium. Journal of Less Common Materials 1964:439.
[34] Klopp W. Review if Ductilizing of Group VIA Elements by Rhenium and Other Solutes. NASA Technical Note. Cleveland: Lewis Research Center, 1968.
[35] Stephens J, Klopp W. Enhanced Ductility in Binary Chromium Alloys. Transactionsof the Metallurgical Society of AIME 1968;242:1837.
[36] Klopp WD. Review of Chromium, Molybdenum, and Tungsten Alloys. Journal of the Less-Common Metals 1975;42:261.

[37] Gao MC, Dogan ON, King P, Rollett AD, Widom M. The first-principles design of ductile refractory alloys. Jom 2008;60:61.
[38] Pugh SF. Relations between the Elastic Moduli and the Plastic Properties of Polycrystalline Pure Metals. Philosophical Magazine 1954;45:823.
[39] Reed-Hill R. Physical Metallurgy Principles. Boston: PWS Publishing Company, 1994.
[40] Kurishita H, Kuwabara T, Hasegawa M. Development of Fine-Grained V-28Cr-2.3Y and V-52Cr-1.8Y Alloys With Superior Mechanical Properties. Materials Science and Engineering A 2006;433:32.
[41] International A. Standrad Test Methods for Determination of Carbon, Sulfur, Nitrogen, and Oxygen in Steel, Iron, Nickel and Cobalt Alloys by Varios Combustion and Fusion Techniques. Metals Test Methods and Analytical Procedures. Conshohocken, PA, 2009. p.611.
[42] Shewmon P. Diffusion in Solids. Warrendale: The Minerals, Metals & Materials Society, 1989.
[43] International A. Standard Test Methid for Vickers Hardness of Metallic Materials. Metals Test methods and Analytical Procedures, vol. E92-82. West Conshohocken, PA: ASTM International, 2010. p.8.
[44] Dieter G. Mechanical Metallurgy. Boston: Mc Graw-Hill, 1986.
[45] International A. Standard Test Method for Flexural Strength of Advanced Ceramics at Ambient Temperature. vol. C1161-02. West Conshohocken, PA: ASTM International, 2010. p.15.
[46] International A. Standard Test Methods for Tension Testing of Metallic Materials. Metals Testing and Analytical Procedures, vol. E8-09. West Conshohocken, PA: ASTM International, 2010. p.65.
[47] Newman JC, Raju IS. An Empirical Stress-Intensity Factor Equation for the Surface Crack. Engineering Fracture Mechanics 1981;15:185.
[48] Smithells Metals Reference Book. In: Gale WF, Totemeier TC, editors: Elsevier, 2004.